https://doi.org/10.5194/egusphere-2025-6013
Preprint. Discussion started: 12 December 2025

Understanding the balance between methane production and oxidation from wetlands using a minimalistic emissions model

Gordon R. McNicol[1], Anita T. Layton[2], and Nandita B. Basu[3]

[1]Department of Applied Mathematics, University of Waterloo, Waterloo, ON, Canada
[2]Department of Applied Mathematics, Department of Biology, Cheriton School of Computer Science and School of Pharmacy, University of Waterloo, Waterloo, ON, Canada
[3]Department of Civil and Environmental Engineering and Department of Earth and Environmental Sciences, University of Waterloo, Waterloo, ON, Canada

Correspondence: Gordon R. McNicol (gordon.mcnicol@uwaterloo.ca)

Abstract. Wetlands play a crucial role in the global carbon cycle, both by sequestering large amounts of carbon in their soils and acting as a major natural source of atmospheric methane. Methane emissions depend strongly on soil temperature, substrate availability, and the depth of the water table relative to the soil surface, reflecting a balance between production, oxidation, and transport. Here we develop a simple mathematical model that captures how production and oxidation interact to control emissions. We condense these processes into a single ordinary differential equation, parameterised by water-table depth, soil temperature, and vegetation-derived carbon inputs, to mechanistically explore how these factors interact to control wetland methane emissions. Using emission data from six mid-latitude wetlands in the Prairie Pothole Region, we show that the model can reproduce seasonal and inter-annual variation in fluxes. Having established this agreement, we employ the model to investigate the conditions under which emissions are maximised. Peak fluxes consistently occur at or just above the soil surface and are strongly modulated by wetland-specific parameters, with oxidation acting as a significant sink in some systems. Importantly, we find that the temperature sensitivity of oxidation is a key determinant of both the magnitude and location of peak emissions. These results highlight how warming may shift emission dynamics, emphasising the need for site-specific and adaptive wetland management and restoration strategies.

1 Introduction

Wetlands are water-saturated ecosystems, typically occurring near lakes, ponds, or rivers. Based on water depth and hydroperiod, they are classified as marshes, swamps, bogs, or fens, with areas spanning a few hectares to several hundred square kilometres (Junk, 2024). Serving as a boundary between land and aquatic environments, these diverse and dynamic ecosystems provide a habitat for a variety of plants, animals, and microbes whilst also performing critical ecological functions such as water filtration, retention, and purification (Bridgham et al., 2006; Zedler and Kercher, 2005). Given this wide array of functions, wetlands are often touted as a possible nature based solution (e.g. for flood prevention Ferreira et al., 2023) and there has been a recent push for their enhanced conservation given their previous loss due to anthropogenic activities, including urbanisation and agricultural intensification (Bradford, 2016; Verhoeven and Setter, 2010).

https://doi.org/10.5194/egusphere-2025-6013
Preprint. Discussion started: 12 December 2025

Wetlands also play a significant role in the global carbon and nitrogen cycles: they sequester large amounts of carbon in their soils, storing around one-third of global soil carbon despite covering only 5–8% of the land area (Mitsch et al., 2013), and emit greenhouse gases (GHGs) through active microbial processes (Bridgham et al., 2006; Salimi et al., 2021). These include carbon dioxide (CO_2), nitrous oxide (N_2O), and methane (CH_4), which is the focus of this paper. Indeed, wetlands, together with inland waters, are responsible for approximately 83% of natural global CH_4 emissions and 22–48% of total CH_4 emissions (Forbrich et al., 2024; Saunois et al., 2019), with those located in tropical and mid-latitudes contributing significantly to the increase in global CH_4 concentrations in recent decades (Forbrich et al., 2024). Given the need to balance the local ecological benefits of wetlands against the global risks of enhanced GHG emissions and their contribution to climate change, improved understanding of emission mechanisms and more accurate estimates of total wetland emissions are required.

Emissions from individual wetlands are shaped by a complex interactions between ecological, hydrological, climatic, and human influences. Amongst these, the position of the water table relative to the soil surface, soil temperature, and the supply of carbon substrates for CH_4 production exert the strongest controls (Moore and Dalva, 1993; Turetsky et al., 2014). These three drivers govern the balance of wetland CH_4 dynamics – methanogenesis (CH_4 production), methanotrophy (CH_4 oxidation), and release to the atmosphere via diffusion, ebullition, or plant-mediated transport. Field measurements of CH_4 fluxes, whether obtained from chamber studies or eddy-covariance systems, therefore capture the net outcome of these competing processes.

In wetland ecosystems, submerged soils provide the anaerobic conditions that favour methanogenesis (Hondula et al., 2021), where alternative electron acceptors are scarce and organic carbon decomposition proceeds slowly (Thauer and Shima, 2008). When the water table drops below the surface, methanogenesis is suppressed and CH_4 oxidation intensifies (Bansal et al., 2016); continued lowering exposes soil carbon pools to fully aerobic conditions, where microbes instead releasing CO_2 through respiration (Le Mer and Roger, 2001; Wu et al., 2024). Hence, water table position marks a demarcation between anaerobic production and aerobic consumption of CH_4 (Segers, 1998). Temperature further modulates both methanogenesis and oxidation through its control of microbial kinetics, accelerating reaction rates with warming, and dampening them when soils cool (Bansal et al., 2016). Meanwhile, vegetation biomass influences all stages of the CH_4 dynamics by supplying carbon substrate through the decomposition of organic matter, transporting oxygen to root zones that enhance local oxidation, and providing conduits for plant-mediated CH_4 emission in addition to diffusion and ebullition pathways (Bansal et al., 2020; Schütz et al., 1991; Stewart et al., 2024). These controls are strongly coupled. For example, soil water balance is governed by ecohydrologic processes such as infiltration, runoff, and evapotranspiration (Cui et al., 2024; Mitsch and Gosselink, 2015), which in turn are influenced by atmospheric and soil temperature as well as vegetation.

A wide range of models have been developed to quantify wetland CH_4 dynamics. At large scales, empirical or data-driven approaches are commonly used and often achieve high predictive accuracy (e.g. Bansal et al., 2023; McNicol et al., 2023; Ying et al., 2024; Yuan et al., 2022). However, because these approaches link environmental drivers (e.g. water table, temperature, vegetation) directly to net emissions, they cannot distinguish the relative contributions of production, oxidation, and emission pathways. Moreover, data-driven models provide only limited mechanistic insight, making it difficult to interpret how or why fluxes respond to changing conditions. In contrast, process-based biogeochemical models such as DNDC (Li, 2000; Zhang et al., 2002; Haas et al., 2013) and ecosys (Grant and Roulet, 2002) provide accurate mechanistic descriptions for simulating

https://doi.org/10.5194/egusphere-2025-6013
Preprint. Discussion started: 12 December 2025

nitrogen and carbon cycling in soils to predict N_2O, CO_2, and CH_4 fluxes. Other models, including the LPJ model (Smith et al., 2001; Wania et al., 2010), focus on the influence of wetland vegetation patterns on emissions, while WETMETH (Nzotungicimpaye et al., 2021) specifically addresses the dependence of emissions on soil moisture. Although they do so with varying degrees of sophistication, these models generally incorporate explicit representations of soil microbial processes (e.g. nitrification, denitrification, fermentation), plant growth and decay (e.g. photosynthesis and litter input), soil properties and hydrology, and carbon-nutrient interactions (for further details see reviews by Forbrich et al., 2024; Melton et al., 2013; Xu et al., 2016). However, despite their sophistication and predictive skill, they are often computationally intensive, require extensive parameterisation, and can make it difficult to isolate the mechanisms most responsible for observed CH_4 fluxes.

To improve interpretability and enable sensitivity analyses, simplified mechanistic models have been developed that focus on the dominant processes driving CH_4 fluxes, often using reduced reaction-diffusion-advection formulations combined with empirical parameterisations (e.g. Arah and Stephen, 1998; Walter et al., 1996; Walter and Heimann, 2000; Tang et al., 2010). A key emergent behaviour from such models is the existence of a critical water depth at which emissions peak, reflecting the balance between production and oxidation. Using a zero-dimensional framework, Calabrese et al. (2021) found a robust peak near 50 cm inundation depth across multiple datasets and wetland types. In their formulation, fluxes from a soil column were determined by CH_4 generation, oxidative loss, and release through diffusion, ebullition, and plant-mediated transport. Whilst the model reproduced observed peaks under inundated conditions (Calabrese et al., 2021; Cui et al., 2024), it was parameterised with fixed water depths and excluded dynamic variation in temperature or substrate supply. As a result, it remains unclear whether the critical depth is universal or instead shifts with drivers such as soil temperature, vegetation biomass, or seasonal hydrologic change.

To explore these questions, we develop a minimal mechanistic model linking water-table depth, soil temperature, and vegetation activity to CH_4 production, oxidation, and emission in wetland soils. The model adapts the framework of Calabrese et al. (2021) and consists of a single ordinary differential equation parameterised by these environmental drivers, validated against growing-season flux observations from mid-latitude wetlands in the Prairie Pothole Region, USA. Our objective is to capture the key drivers of emission seasonality, determine how they jointly control the magnitude of peak CH_4 fluxes, and how the balance between production and oxidation sets the water depth at which this peak occurs. By focusing on a single, interpretable equation that captures the dominant processes, we provide a simple yet robust framework for predicting wetland CH_4 emissions under variable hydrologic and climatic conditions.

2 Mathematical model

We represent the wetland as a collection of vertical one-dimensional soil columns. Each column is defined over the vertical coordinate z in the domain $z_b \leq z \leq z_s$, where $z = z_s$ denotes the soil surface and $z = z_b$ the soil base (see Fig. 1a). The water table lies at $z = z_w(t)$, which may rise above z_s under inundated conditions. Henceforth, we focus on soil columns at the centre of each wetland and neglect lateral exchanges with adjacent columns. All processes of interest are therefore resolved only in the vertical direction. This assumption is justified as chamber-based flux measurements inherently reflect local conditions,

https://doi.org/10.5194/egusphere-2025-6013
Preprint. Discussion started: 12 December 2025

supporting a column-wise modelling approach focused on vertical processes. Our subsequent analysis concentrates on the vertical dynamics of a representative soil column located at the wetland centre.

2.1 Model overview

We employ a simple ODE model to describe CH_4 emission from the soil column, accounting for the competing influence of methanogenesis and methanotrophy. We denote by M_s (mg CH_4 cm^{-2}) the total mass of CH_4 in the soil column per unit ground area. Methane is produced in the soil column at rate f_p (mg CH_4 m^{-2} d^{-1}), oxidised at rate f_o (mg CH_4 cm^{-2} d^{-1}), and emitted via plant transport, ebullition, and diffusion at rate f_e (mg CH_4 cm^{-2} d^{-1}). Hence, the CH_4 dynamics in soil can be summarised as

$$\frac{dM_s}{dt} = f_p - f_o - f_e, \tag{1}$$

where the reaction and transport terms are parameterised by the water table depth, soil temperature and availability of carbon substrate due to plant biomass (in a similar manner to Gedney et al., 2004; Walter and Heimann, 2000). Figure 1 illustrates how CH_4 production, oxidation, and emission respond to these key environmental drivers.

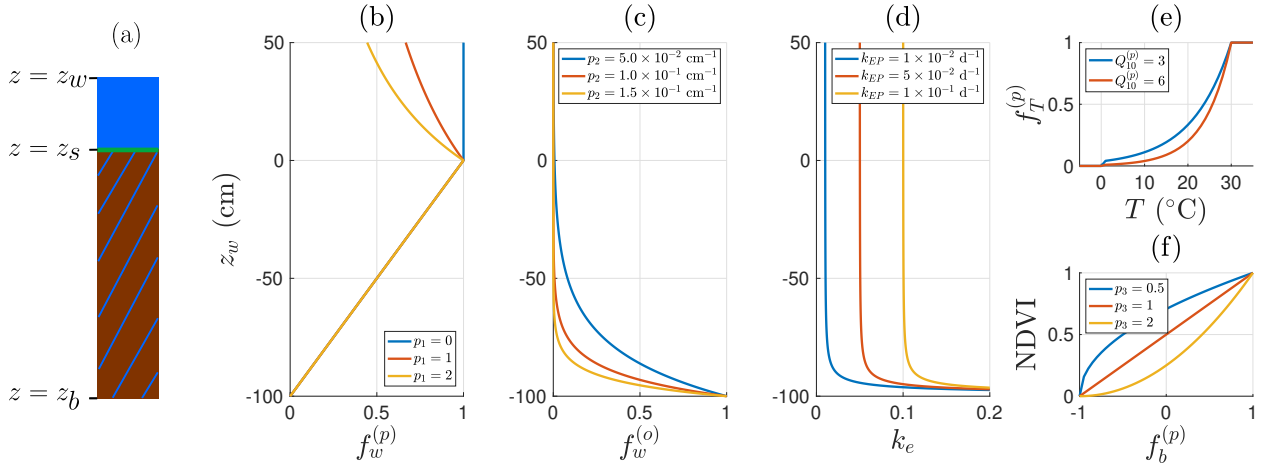

Figure 1. Model geometry and assumed functional dependencies of environmental drivers. (a) Schematic of the wetland soil column showing z_b, z_s, and z_w. Functional dependence of (b) methane production, (c) oxidation, and (d) emission fluxes on water depth where $z_b = -100$ cm, $z_s = 0$ cm and $z_w > 0$ cm. Production dependence on (e) soil temperature and (f) NDVI.

2.2 Methane production

Wetland methanogenesis is governed by three primary environmental drivers: water table depth, soil temperature, and the availability of carbon substrate (Bridgham et al., 2013). Hence, we assume that the rate of CH_4 production in the soil column

https://doi.org/10.5194/egusphere-2025-6013
Preprint. Discussion started: 12 December 2025

is given by

$$f_p = k_p f_b^{(p)} f_T^{(p)} f_w^{(p)}, \tag{2}$$

where k_p (mg CH_4 cm^{-2} d^{-1}) is a calibrated constant for each wetland, and the terms $f_b^{(p)}$, $f_T^{(p)}$, and $f_w^{(p)}$ are dimensionless scaling functions representing, respectively, the availability of carbon substrate due to plant biomass decay, the temperature dependence of methanogenesis, and the effect of water table depth on methanogenesis.

Methanogenesis occurs in the anoxic layers of the soil and is therefore strongly dependent on water table depth. When the water table lies below the soil surface, higher water table depths increase the anoxic zone, promoting CH_4 production. However, waterlogged conditions can reduce CH_4 production by diluting dissolved organic substrates in the soil, lowering their concentration and thus limiting methanogenesis. As illustrated in Fig. 1(b), we use the same piecewise water table dependence as Calabrese et al. (2021). In particular, we have

$$f_w^{(p)} = \begin{cases} \left(\frac{z_w - z_b}{z_s - z_b}\right), & z_w < z_s \\ \left(\frac{z_w - z_b}{z_s - z_b}\right)^{-p_1}, & z_w \geq z_s \end{cases}, \tag{3}$$

where $0 \leq f_w^{(p)} \leq 1$ (see Fig. 1a). The exponent $p_1 \geq 0$ characterises CH_4 production in the region below the water table but above the soil column; $p_1 = 0$ corresponds to no mixing of carbon substrate, whereas $p_1 \gg 0$ corresponds to well-mixed conditions. In other words, CH_4 production increases linearly with water table depth as the anoxic zone expands, such that $f_w^{(p)} = 0$ when the water table lies at the base of the soil column and $f_w^{(p)} = 1$ at the soil surface. Beyond the soil surface, further inundation reduces production, following a negative power-law relationship with $f_w^{(p)} \to 0$ as $z_w \to \infty$.

Two methanogenic pathways typically dominate in wetlands: hydrogenotrophic, whereby bacteria reduce CO_2 with hydrogen to form CH_4; and acetoclastic, in which bacteria convert acetic acid from decomposing organic matter into both CH_4 and CO_2 (Conrad, 1999; Thauer et al., 2008). Biomass availability thus plays a crucial role in both pathways – directly through litter input for acetoclastic methanogenesis, and indirectly via CO_2 production for hydrogenotrophic methanogenesis. Despite differences between these pathways, for simplicity we combine them into a single effective methanogenesis term. To represent this dependence, we use the Normalised Difference Vegetation Index (NDVI) as a proxy for available plant biomass. NDVI, which ranges from -1 to 1, quantifies vegetation density and health based on the differential reflectance between near-infrared and red light, typically derived from satellite data. To account for the lag between vegetation growth and availability of decomposable organic matter, we introduce a delay τ days between NDVI and biomass availability (see Bansal et al., 2023), such that

$$f_b^{(p)} = \left(\frac{1 + \mathrm{NDVI}(t - \tau)}{2}\right)^{p_3}, \tag{4}$$

where $p_3 \geq 0$ (see Fig. 1f). This functional form ensures that $0 \leq f_b^{(p)} \leq 1$.

Soil temperature strongly regulates both major CH_4 production pathways through temperature-dependent enzyme kinetics (Yvon-Durocher et al., 2014). This influence is two-fold: higher temperatures enhance fermentation processes such as increased

https://doi.org/10.5194/egusphere-2025-6013
Preprint. Discussion started: 12 December 2025

root exudation, and directly stimulate methanogen activity. The temperature dependence of methanogenesis typically follows an Arrhenius-type (i.e. exponential) relationship (Dunfield et al., 1993). Following previous models (e.g. Souza et al., 2021; Walter and Heimann, 2000), we represent this effect using a Q_{10} formulation:

$$f_T^{(p)} = \begin{cases} 0, & T \leq 0°\mathrm{C} \\ Q_p^{\frac{1}{10}(T-30)}, & 0°\mathrm{C} < T < 30°\mathrm{C} \\ 1, & T \geq 30°\mathrm{C} \end{cases}, \tag{5}$$

where T (°C) is the soil temperature, $Q_p \geq 1$ is a fitted parameter, and $0 \leq f_T^{(p)} \leq 1$ (see Fig. 1e). This form reflects enzymatic saturation above an optimal temperature, which we set at 30°C due to the mid-latitude wetland focus, where temperatures rarely exceed this threshold.

2.3 Methane oxidation

Methane produced in the soil column may be oxidised before reaching the surface, thereby preventing its emission into the atmosphere. This oxidation occurs predominantly under aerobic conditions in the unsaturated soil zone and is therefore strongly modulated by the position of the water table. Additionally, soil temperature regulates the activity of methanotrophic bacteria (Segers, 1998).

We refine the model of Calabrese et al. (2021) by assuming that CH_4 oxidation follows first-order reaction kinetics that depend on water-table depth (*cf.* CH_4 production, which is treated as a zero-order process, reflecting that methanogenesis is primarily controlled by substrate availability rather than the instantaneous CH_4 concentration within the soil column). In our formulation, oxidation is further modified by temperature through a multiplicative factor, such that

$$f_o = k_o f_T^{(o)} f_w^{(o)} M_s, \tag{6}$$

where k_o (d^{-1}) is the maximum oxidation rate under atmospheric oxygen availability throughout the soil column; $f_T^{(o)}$ and $f_w^{(o)}$ are dimensionless functions describing the dependence of methanotrophy on soil temperature and water table depth, respectively. For simplicity, oxygen transport via plant roots, which could enhance methanotrophy, is neglected here.

Following Calabrese et al. (2021), we model the water table dependence of oxidation as an exponential decay with increasing water table depth:

$$f_w^{(o)} = e^{-p_2(z_w - z_b)}, \tag{7}$$

where $p_2 > 0$ (cm^{-1}) is a control parameter (see Fig. 1c). Thus, oxidation is maximal when the water table is at the base of the soil column ($z_w = z_b$) and decreases sharply as the water table rises. To capture temperature dependence, we employ a Q_{10} relationship analogous to that used for CH_4 production (e.g. Walter and Heimann, 2000):

$$f_T^{(o)} = \begin{cases} 0, & T \leq 0°\mathrm{C} \\ Q_o^{\frac{1}{10}(T-30)}, & 0°\mathrm{C} < T < 30°\mathrm{C} \\ 1, & T \geq 30°\mathrm{C} \end{cases}, \tag{8}$$

https://doi.org/10.5194/egusphere-2025-6013
Preprint. Discussion started: 12 December 2025

where $Q_o \geq 1$ is a constant.

2.4 Methane emissions

Methane produced in the soil column is emitted into the atmosphere by three distinct mechanisms: diffusion, plant transport and ebullition. We assume emission by diffusion occurs at rate k_D (d^{-1}), emission due to plant transport at rate k_{PT} (d^{-1}), and emission due to ebullition at rate k_{EB} (d^{-1}). We employ a simple functional form (see Fig. 1d) for CH_4 emission:

$$f_e = k_e M_s, \quad k_e = k_D + k_{EB} + k_{PT}. \tag{9}$$

Emission is treated as first-order, dependent on the total soil CH_4 pool. Such a simple form neglects the vertical motion of CH_4 (e.g. detailed in models by Walter et al., 1996; Zhang et al., 2002) but has been demonstrated to successfully describe key aspects of CH_4 emission (Calabrese et al., 2021).

Diffusive release involves CH_4 movement down gradients from regions of high CH_4 concentration in the anaerobic soil to the atmosphere. This transport is slow and subject to methanotrophic oxidation, but typically dominates when soils are moist or water columns are deep and oxygenated. The effectiveness of diffusion decreases with water table depth, since the diffusive path lengthens and so the rate of diffusive release scales inversely. Hence, the rate of diffusive transport of CH_4 is given by

$$k_D = \frac{D}{(z_w - z_b)^{p_4}}, \tag{10}$$

where D is the diffusion coefficient of CH_4 and $p_4 = 2$ for Fickian diffusion. Soil temperature can provide an additional layer of complexity, by affecting water viscosity and gas diffusion, though we neglect this.

Meanwhile, plant transport and ebullition provide more efficient emission routes. In the case of plant transport, CH_4 travels along gas conduits (e.g. roots, stems) in arenchymous plants or tree stems by means of convective flow, molecular diffusion, or pressure-driven transport (Joabsson et al., 1999). This allows CH_4 to bypass much of the (aerobic) oxidation zone, preventing methanotrophy (Laanbroek, 2010). As such, plant transport is largely independent of water table depth (though this can still influence plant rooting depth and wilting) and can play a dominant role in vegetated wetlands, particularly during peak growing season. On the other hand, ebullition provides a sporadic emission mechanism due to bubbling of supersaturated CH_4. These emission pulses bypass methanotrophy almost entirely and are triggered when gas pressure overcomes surface tension, typically in response to fluctuations in hydrostatic or atmospheric pressure, or changes in temperature (Walter et al., 2006). We assume, in an identical manner to Calabrese et al. (2021), that plant transport and ebullition occur at a constant rate, which for the remainder of this paper we couple into one term, $k_{EP} = k_{EB} + k_{PT}$. However, future model refinements could link plant transport to NDVI, and ebullition to changes in weather conditions and water table depth.

2.5 Computational method

We solve the single ODE (1) in MATLAB using the inbuilt stiff solver `ode15s` and employ default error tolerances. The results are well converged, even for long simulation times. Model parameters are calibrated to individual wetlands by minimising the normalised root mean square error (nRMSE) between observed (oF_i) and predicted (pF_i) CH_4 flux at each data point

https://doi.org/10.5194/egusphere-2025-6013
Preprint. Discussion started: 12 December 2025

$i = 1, 2, \ldots, N$, defined as

$$\text{nRMSE} = \text{RMSE}/\sigma, \quad \text{RMSE} = \sqrt{\frac{\sum_{i=1}^{N} (pF_i - oF_i)^2}{N}}, \tag{11}$$

where σ is the standard deviation of observed fluxes. This normalisation facilitates comparison of model performance across wetlands with differing flux magnitudes (Wania et al., 2010). Following Calabrese et al. (2021), the effective diffusivity of CH_4 in the soil is set as $D = 1.3$ cm^2 d^{-1} in all simulations.

To identify the set of optimised parameters for a particular wetland, we use the inbuilt MATLAB genetic algorithm (`ga`), a population-based, stochastic global optimisation method. This algorithm is particularly suited for solving non-linear and discontinuous optimisation problems where gradient-based methods struggle to converge or become trapped in local minima. In particular, we minimise the nRMSE between model output and observations by calling `ga`, which searches the global parameter space, with possible parameter ranges as detailed in Table A2, until certain convergence criteria are met.

3 A case study

To assess the ability of our model to capture both seasonal and inter-annual variability in CH_4 emissions, we calibrate model parameters using observational data from mid-latitude wetlands. These ecosystems are significant CH_4 sources and exhibit strong climatic variability, particularly in temperature and precipitation (Bridgham et al., 2013). We concentrate on wetlands within the PPR of North America, a region which spans approximately 900,000 km^2 and encompasses portions of Alberta, Saskatchewan and Manitoba in Canada, and Montana, North and South Dakota, Minnesota, and Iowa in the United States (Mushet et al., 2022). This area is characterised by a large population of small, shallow, depressional wetlands formed during glacial retreat more than 10,000 years ago and exhibit highly seasonal hydrological microbial dynamics (Eisenlohr, 1972).

We focus on the Cottonwood Lake Study Area (CLSA) of the PPR, located in Stutsman County, North Dakota. The CLSA wetlands typically contain clay-rich soils, interspersed with pockets of sand and silt; the surrounding upland consists of hummocky hilltops and native grassland vegetation (Mushet et al., 2022). The 20 wetlands within the CLSA can be broadly classified based on their hydroperiod with 11 permanent (P1–P11) and 9 temporary (T1–T9) wetlands; wetlands P1–P9 and T1–T9 are shown in Fig. 2. Such a classification allows for the model to be tested across different wetland regimes that typically form different parts of the wetland continuum (Euliss Jr et al., 2014). The permanent wetlands typically retain water year-round (except during severe drought). Most are closed basins, accumulating solutes over time, with only P3 and P8 regularly overflowing. Wetlands P2 and P7 appear hydraulically isolated, except for possible subsurface flows. These features, together with long water residence times and recharge from surrounding wetlands, mean many of these wetlands exhibit high sulphate concentration, suppressing methanogenesis via competitive sulphate reduction (Dalcin Martins et al., 2017). Larger surface-area-to-perimeter ratios in these wetlands may further reduce emissions. In contrast, the CLSA temporary wetlands typically dry out during the summer season and exhibit pronounced seasonal variability (Stewart and Kantrud, 1971). These wetlands (with the exception of T1 and T9) are open basins that overflow during high-water events, limiting the maximum water depth and promoting discharge to surrounding wetlands. Their repeating filling (by rainfall) and draining leads to fresher conditions

https://doi.org/10.5194/egusphere-2025-6013
Preprint. Discussion started: 12 December 2025

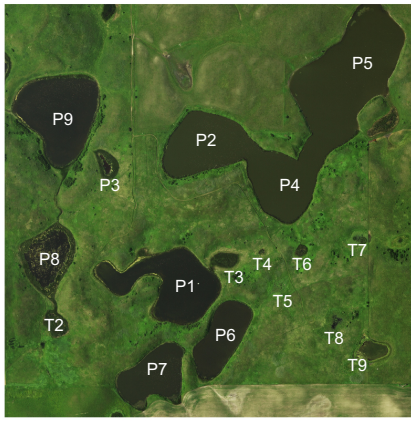

Figure 2. Cropped RGB satellite image centred on the CLSA (P10–P11 not shown). Image is derived from National Agriculture Imagery Program (NAIP) aerial imagery acquired on 20 July 2014, accessed via the USGS EarthExplorer platform (U.S. Geological Survey, 2014). Image has been rescaled and spatially cropped for clarity. Source: NAIP, U.S. Geological Survey (public domain).

and lower salinity, amplified by the low hydraulic conductivity characteristic of the PPR wetlands (Richardson et al., 1994). This wetland heterogeneity makes the CLSA an ideal testing site for our model performance.

3.1 Parameter ranges and fitting

We fit model parameters for each wetland using the dataset provided by Bansal et al. (2023), which includes data at approxi-
230 mately fortnightly (occasionally coarser) intervals for NDVI, soil temperature, water depth, water-filled pore space (WFPS) at the soil surface and CH_4 flux throughout the growing season (April–November). To reduce bias from extreme outliers in CH_4 flux measurements, likely caused by ebullition or anthropogenic disturbance, we exclude data points where CH_4 fluxes exceed 20 times the interquartile range for each wetland. The possible parameter ranges for each wetland are given in Table A2 in App. A, based on an extensive review of the literature.

235 When the water table lies above the soil surface, direct measurements of water depth are available. For periods when the water table falls below the surface, observed water depths are truncated at 0 cm, so subsurface positions must be estimated. For simplicity, to estimate z_w when the water table is below the surface, we assume a linear relationship with WFPS. Zero water depth measurements are replaced with these estimates and capped at $z_w = -49.9$ cm to remain within the model domain. This approach neglects lateral flow and potential time lags between water table changes and CH_4 emissions, but provides a
240 first-order seasonal estimate adequate for budget calculations, which are usually dominated by periods when the water table is at or above the soil surface.

In order to force our model at the daily scale, we linearly interpolate between observations for all model drivers, i.e. NDVI, soil temperature, water depth and WFPS (a similar approach is employed by Walter and Heimann, 2000). We also introduce "ghost" data points two weeks before and after the observed growing season for each year, assuming $T = 0\,°C$ and $F = 0$ mg

https://doi.org/10.5194/egusphere-2025-6013
Preprint. Discussion started: 12 December 2025

CH_4 cm^{-2} d^{-1} (i.e. no CH_4 flux) to reflect dormancy in the winter, whilst holding NDVI and water table depth constant in this two week period. As discussed in Sect. 2, NDVI is introduced as a calibrated time-lagged forcing term, using values from τ days prior to account for the delay between photosynthetic activity and substrate availability due to plant growth and litter decomposition. Note that observed total CH_4 emissions are estimated by linearly interpolating daily flux measurements and numerically integrating them over each seasonal period.

4 Results

4.1 Model performance

To assess how well the model captures observed emission patterns, Figs. 3–4 show baseline simulations using optimised parameters derived using the method described in Sect. 2.5 (see Table A1 for details). In particular, Fig. 3 compares modelled CH_4 fluxes (blue line) with observations (red crosses) for the 2009–2016 growing seasons (note that Bansal et al., 2023, provide data for wetland T5 only through 2015). The corresponding cumulative emissions are presented in Fig. 4, where predicted (blue) and observed (red) totals show close agreement. Panels (a)–(f) correspond to wetlands P1, P3, P8, T5, T6, and T9, respectively, spanning permanent and temporary types and representing a range of hydrological settings (Euliss Jr et al., 2014): three recharge wetlands (P3, T5, T6), one discharge (P1), one flow-through (P8), and one apparently hydrologically isolated site (T9). The full response to modelled environmental drivers are detailed in Sect. S1 of the supplementary material.

The data reveal a clear positive correlation between CH_4 fluxes and both soil temperature and NDVI, which overall the model reproduces well. Emissions typically peak in mid- to late-growing season (July–September), when temperatures are highest and plant deterioration begins, demonstrating the importance of including these environmental drivers. The model captures the major flux dynamics, responding realistically to both soil temperature and vegetation activity, and also reproduces the near-zero CH_4 emissions observed in early spring and late autumn, when low temperature and limited substrate constrain methanogenesis. Meanwhile, the relationship between emissions and water-table depth is more complex (see Sect. 5.3 below). Variations in water level influence CH_4 production, oxidation, and transport not only directly, but also indirectly by changing factors such as wetland salinity or the concentration of alternative electron acceptors. These effects contribute to the significant heterogeneity in peak fluxes between wetlands. In particular, field observations indicate temporary wetlands generally exhibit higher emissions (Mushet et al., 2022).

Focusing first on the permanent wetlands, model performance is strong for wetland P1 (Fig. 3a), particularly during the 2009, 2010, 2015, and 2016 growing seasons. In 2015 the model captures two distinct seasonal emission peaks that align with observed soil-temperature maxima, reflecting its sensitivity to temperature forcing. Wetland P3 likewise demonstrates the need for the additional environmental drivers: during the 2010, 2011, and 2015 seasons, water depth remains nearly constant early in the year whilst emissions increase in tandem with lagged NDVI and temperature. Moreover, rare anomalously high CH_4 fluxes outside this window often coincide with elevated lagged NDVI or temperature, such as the early 2012 peak (Fig. 3b), driven by a large carbon substrate pool (see Fig. S1f in the supplementary material). Performance for wetland P8 is more mixed. The model generally reproduces the overall pattern of low spring and autumn fluxes and higher summer emissions, together with

https://doi.org/10.5194/egusphere-2025-6013
Preprint. Discussion started: 12 December 2025

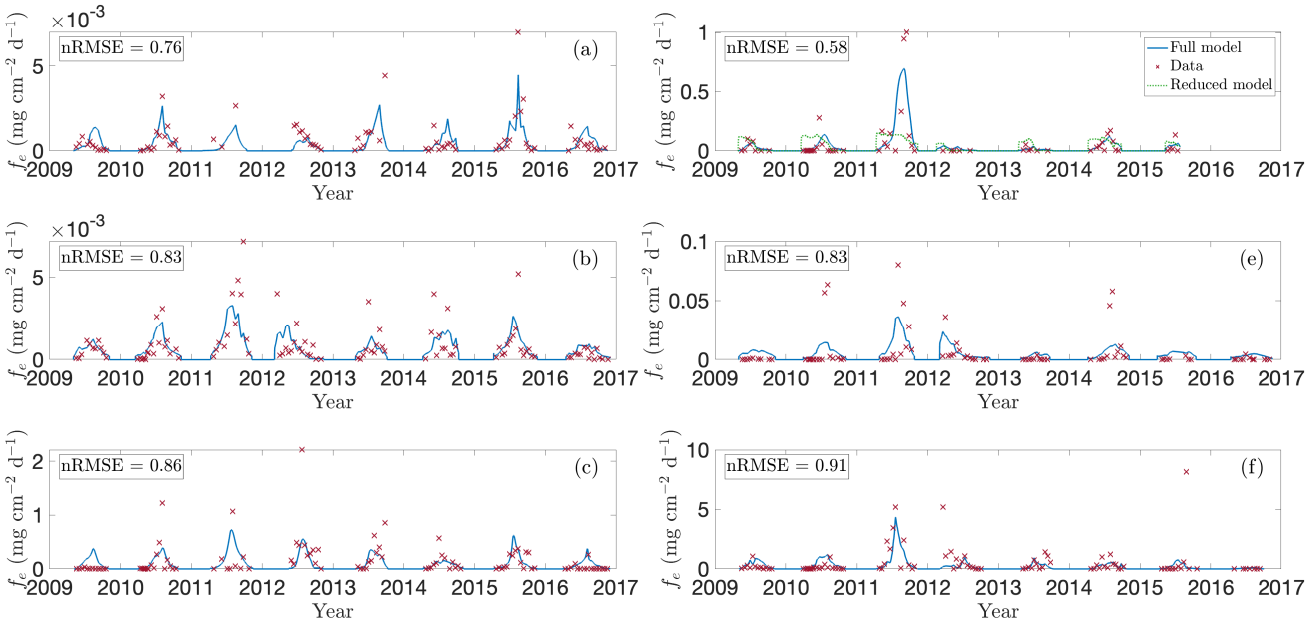

Figure 3. Model predictions versus observed CH_4 fluxes for selected wetlands in the CLSA. Panels show modelled (blue lines) and observed (red crosses; data from Bansal and Tangen, 2022) growing-season fluxes (2009–2016) for wetlands (a) P1, (b) P3, (c) P8, (d) T5, (e) T6, and (f) T9. These sites were chosen to represent the range of wetland types – permanent, temporary, source, sink, and flow-through. In panel (d), the green line shows predictions without temperature and NDVI dependence, corresponding to the framework of Calabrese et al. (2021).

the early 2012 peak, but performs poorly in 2009 and 2011. During both years emissions remain unexpectedly low despite favourable temperatures, water depths, and typical vegetation growth, leading the model to overestimate total seasonal fluxes (Fig. 4c). This discrepancy may reflect additional hydrological complexities: as a flow-through wetland, P8 may experience transient salinity or redox dynamics not represented in the model.

Overall, the model also performs well for the temporary wetlands, particularly for wetland T5 (Fig. 3d), where it correctly capturing the trend in each season and reproduces the pronounced peak in CH_4 emissions during the 2011 growing season (in response to elevated soil temperatures, see Fig. S4e in the supplementary material). Moreover, the model replicates muted emissions in 2012, when the water table remained below the soil surface (Fig. S4d in the supplementary material). This clearly demonstrates the modulating influence of water table depth; for example, unlike in wetland P3, emissions in T5 do not appreciably rise early in 2012 despite anomalously early plant growth (Fig. S4f in the supplementary material). Results are more mixed for wetland T6 (Fig. 3e) but relatively strong for wetland T9 (Fig. 3f). In 2012 both wetlands also experienced unusually early plant growth; in T6, the model correctly captures the peak emissions in April–May, followed by a decline. In both T6 and T9, the model captures the high summer 2011 fluxes, driven by elevated soil temperatures (Figs. S5e, S6e in the supplementary material). Meanwhile, for T9 the model reproduces negligible 2016 emissions, attributable to low water table, cooler soil, and limited substrate, but it misses a sharp late-season spike in 2015. Excluding this outlier substantially reduces

https://doi.org/10.5194/egusphere-2025-6013
Preprint. Discussion started: 12 December 2025

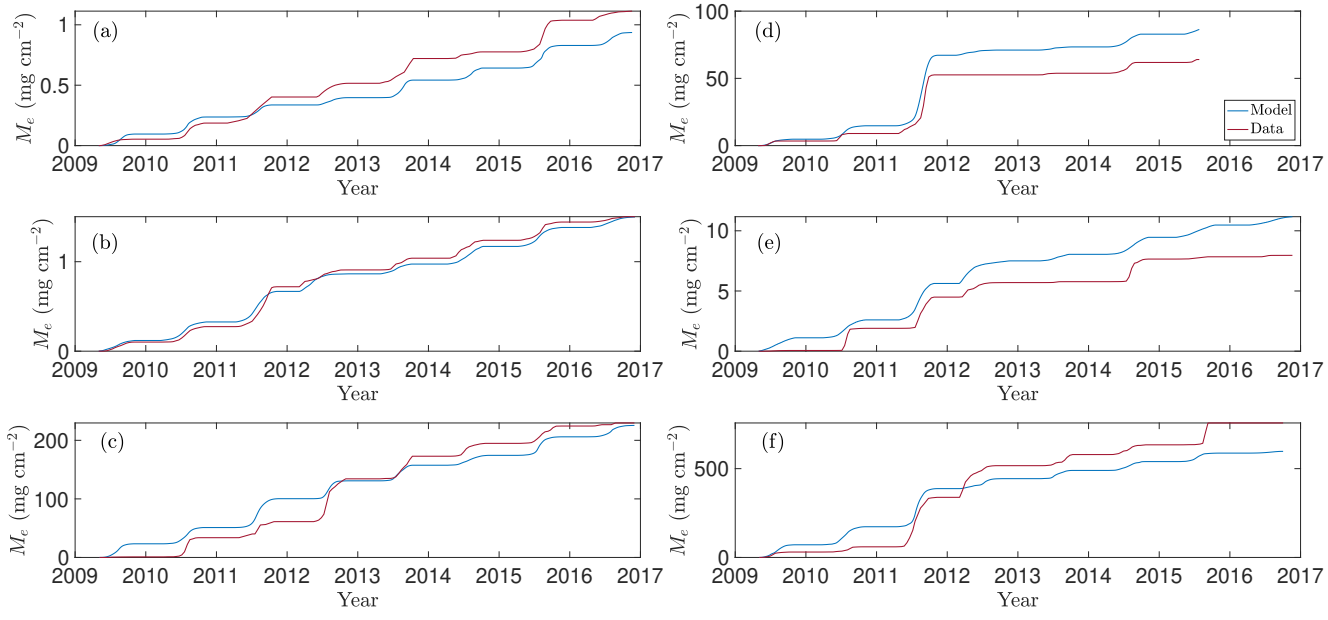

Figure 4. Model predictions versus approximate total observed CH_4 emissions for selected wetlands in the CLSA. Panels show modelled (blue line) and approximate observed (red line; based on data from Bansal and Tangen, 2022) total CH_4 emissions for wetland centres over the growing seasons 2009-2016 for wetlands (a) P1, (b) P3, (c) P8, (d) T5, (e) T6, and (f) T9.

the nRMSE, making T9 one of the best-described sites overall. The 2015 spike coincides with a rapid water-table drop and is likely due to ebullition or enhanced diffusion, suggesting the need for more detailed representation of these processes in future model iterations.

In Fig. 3(d) we also compare our full model with the reduced Calabrese et al. (2021) formulation, demonstrating the benefit of including vegetation and temperature drivers. Focusing on wetland T5, the framework of Calabrese et al. (2021) capably describes steady-state behaviour, but fails to reproduce the strong seasonal variability in CH_4 fluxes. Incorporating a Q_{10} temperature dependence for methanogenesis and oxidation substantially improves the timing and magnitude of predicted emissions, highlighting the dominant role of temperature under inundated conditions. Yet temperature alone cannot explain all observed fluctuations. Including NDVI as an independent proxy for substrate availability is crucial, particularly in reproducing anomalous early-season peaks such as those in various wetlands in 2012. Given the central roles of temperature and substrate availability, we also tested whether including water-table depth improves model performance (results not shown). For permanent wetlands, which typically remained inundated, the effect is minor, consistent with the optimised parameters in Table A1 that indicate a weak exponential decay of oxidation and a near-zero depth dependence of methanogenesis. In contrast, the influence of water-table depth is much stronger in temporary wetlands, where CH_4 emissions drop sharply once the water table falls below the soil surface.

https://doi.org/10.5194/egusphere-2025-6013
Preprint. Discussion started: 12 December 2025

We further assess model performance in Fig. 5, which also compares predicted and observed CH_4 emissions for each wetland during the 2009–2016 growing seasons. In particular, we present a scatter plot comparing total seasonal emissions in each wetland, perfect model agreement would place data points on the 1:1 grey reference line (i.e. the predicted and observed emissions are equal). At the daily scale, model performance is generally reasonable but shows a consistent bias toward overestimating low emissions, a pattern most evident in temporary wetlands where the water table frequently drops below the surface. However, because these low-flux periods contribute little to the seasonal CH_4 budget (except for brief spikes as the water table falls), integrated emissions remain generally well captured. Indeed, seasonal totals are reproduced reasonably for both permanent and temporary wetlands, including high-emission years such as T9 in 2011, though the model occasionally underestimates emissions when large, infrequent flux events occur and overestimates in years with persistently low observed fluxes (Fig. 5). Performance is notably stronger in permanent wetlands, where water levels typically remain above the surface and fluxes are more stable.

Wetland	Area (m^2)
P1	58,200
P3	6,100
P8	25,100
T5	2,300
T6	1,600
T9	11,500

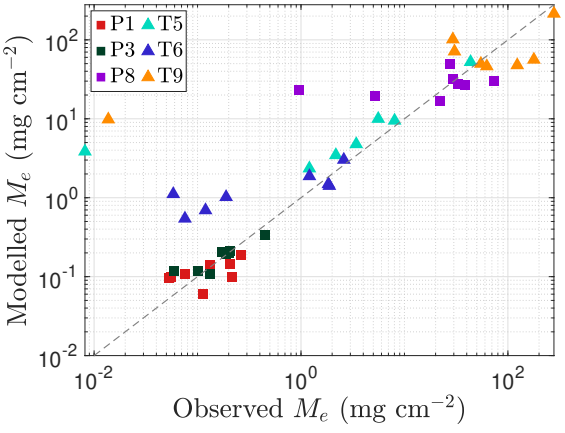

Figure 5. Assessment of model performance in capturing methane (CH_4) emissions from each wetland (P1, P3, P6, P8, T5, T6, and T9) during the 2009–2016 growing seasons. Scatter plot of approximate total observed emissions ($x-$axis; based on data from Bansal and Tangen, 2022) versus total predicted emissions ($y-$axis) for each wetland in each growing season from 2009 to 2016. Permanent wetlands are indicated with squares and temporary wetlands with triangles. The grey line in both panels represents the line of perfect agreement between observations and predictions. Inundated areas for each wetland are listed in the table on the left.

Overall, it is clear from Figs. 3–5 that the model captures the dominant seasonal and inter-annual trends in CH_4 fluxes driven by vegetation, hydrology, and temperature. As expected, a model of this simplicity cannot reproduce every short-term fluctuation. Temperature and hydrology alone explain only about 75–90% of the observed variability in emission dynamics (Bansal et al., 2016), and additional processes (e.g. rainfall-driven dilution of electron acceptors) may further modulate methanogenesis (represented here through the parameter k_p). However, because these higher-frequency fluctuations tend to average out, the model still predicts total seasonal emissions well (Figs. 4, 5), even in years when individual daily fluxes are less accurately captured (e.g. 2013–2014 for wetland P3). This reflects a broader modelling trade-off: whilst low-dimensional ODE models are

https://doi.org/10.5194/egusphere-2025-6013
Preprint. Discussion started: 12 December 2025

tractable, interpretable, and suitable for large-scale projections, they are inherently limited in representing abrupt or non-linear dynamics that govern short-term CH_4 variability.

4.2 Balance between methanogenesis and methanotrophy

Our model also highlights how the role of oxidation differs between temporary and permanent wetlands. Figure 6 shows, for each wetland – a) P1, (b) P3, (c) P8, (d) T5, (e) T6, and (f) T9 – the fraction of CH_4 produced over a season that is emitted, oxidised, or retained in the soil. As expected, oxidation is more significant in temporary wetlands, where water tables frequently fall below the soil surface, allowing CH_4 to be rapidly oxidised before it escapes. In contrast, in permanent wetlands, oxidation is weaker, and in some years, a large fraction of CH_4 produced is emitted rather than consumed. This difference reflects how hydrology controls oxygen availability in the soil: lower water tables increase aeration and microbial access, enhancing oxidation, whereas consistently inundated soils remain largely anoxic. These results emphasise that the balance between production and oxidation, which determines net emissions, is highly sensitive to seasonal water-table dynamics, with implications for wetland management and greenhouse-gas mitigation, including the potential role of repeated drainage in oxidising CH_4 trapped in the soil column. Moreover, the fraction of CH_4 oxidised in the soil column relative to that emitted generally decreases with increasing soil temperature. In most wetlands considered, soil water temperatures peaked in 2011, coinciding with the largest fraction of CH_4 emitted. This pattern arises from the weaker Q_{10}-dependence of oxidation compared with production: as temperatures rise, CH_4 production increases not only in absolute terms but also relative to oxidation, thereby enhancing net emissions.

5 Water depth corresponding to maximum emissions

A key contribution of the model developed by Calabrese et al. (2021) was the ability to capture a critical water depth (≈ 50 cm above the surface) at which CH_4 emissions are maximised due to the interaction between production, oxidation and transport. Given that our model builds upon their framework, we similarly observe this emergent behaviour, with emissions typically suppressed under both drought and deep inundation. To understand the mechanistic origin and parametric sensitivity of this peak, we examine the steady-state behaviour of the system. Our interpretations of this steady-state are applicable more generally: the governing ODEs for CH_4 dynamics are linear in the CH_4 pool size (Eq. 1) and so the qualitative dependence of emissions on water table depth is partly preserved even at intermediate times. However, this is not always the case – the qualitative behaviour can vary over the time-course of a solution, with the depth at which emissions peak becoming time-dependent depending on input parameters and initial conditions – we defer a detailed exploration of this to future work.

Assuming fixed environmental conditions, the system tends towards a steady-state in the soil column, this corresponds to constant emission fluxes from the soil column (see Eq. 9). The steady-state CH_4 mass in the soil column, M_s^*, is obtained by setting $dM_s/dt = 0$ in Eq. (1). Denoting the corresponding emission flux by f_e^*, we have

$$f_e^* = k_e M_s^*, \quad M_s^* = \frac{k_p f_b^{(p)} f_T^{(p)} f_w^{(p)}}{k_o f_T^{(o)} f_w^{(o)} + k_e}. \tag{12}$$

https://doi.org/10.5194/egusphere-2025-6013
Preprint. Discussion started: 12 December 2025

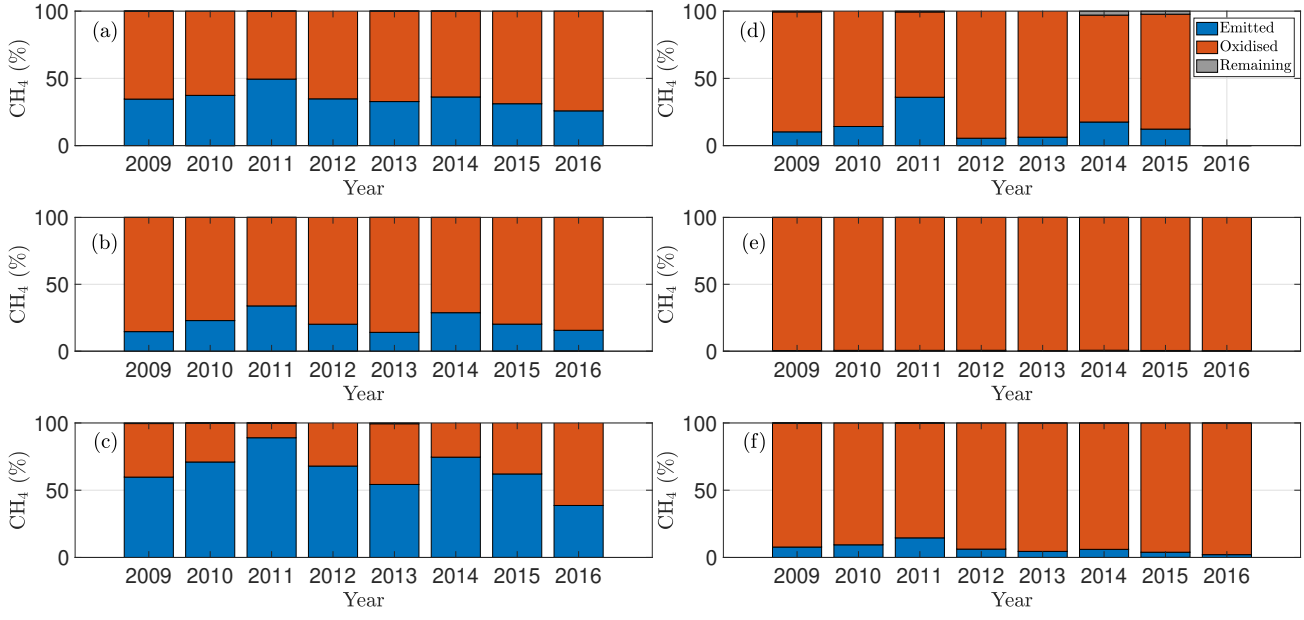

Figure 6. Model predictions of the partitioning of soil CH_4 production into emission, oxidation, and retention over the course of each growing season (2009–2016) for wetlands (a) P1, (b) P3, (c) P8, (d) T5, (e) T6, and (f) T9.

Alternatively, we may write the steady-state emissions as

$$f_e^* = f_p^* - f_o^*, \tag{13}$$

with f_p^* and f_o^* denoting the corresponding production and oxidation rates under fixed environmental conditions. Expressing the system in this form highlights that emissions arise from the balance between production and oxidation, with their differing dependences on environmental conditions giving rise to emergent emission behaviour.

5.1 Dependence of emissions on water table depth

From Eq. (12), f_e^* clearly depends on both the water table depth, and so the location of the emission peak for each wetland depends on the wetland-specific parameters. To identify the water depth z_p that maximises emissions (for a given set of parameters, temperature and substrate availability), we solve for the critical point where $df_e^*/dz_w = 0$. In particular, we have

$$\frac{k_p f_b^{(p)} f_T^{(p)}}{\left(k_o f_T^{(o)} f_w^{(o)} + k_e\right)^2} \left\{ f_w^{(p)} \frac{dk_e}{dz_w} \left(k_o f_T^{(o)} f_w^{(o)} + k_e\right) + k_e \left[\frac{df_w^{(p)}}{dz_w} \left(k_o f_T^{(o)} f_w^{(o)} + k_e\right) - f_w^{(p)} \left(k_o f_T^{(o)} \frac{df_w^{(o)}}{dz_w} + \frac{dk_e}{dz_w} \right) \right] \right\} = 0, \tag{14}$$

https://doi.org/10.5194/egusphere-2025-6013
Preprint. Discussion started: 12 December 2025

which simplifies to

$$f_w^{(p)}\frac{dk_e}{dz_w}\left(k_o f_T^{(o)} f_w^{(o)} + k_e\right) + k_e\left[\frac{df_w^{(p)}}{dz_w}\left(k_o f_T^{(o)} f_w^{(o)} + k_e\right) - f_w^{(p)}\left(k_o f_T^{(o)}\frac{df_w^{(o)}}{dz_w} + \frac{dk_e}{dz_w}\right)\right] = 0. \tag{15}$$

Hence, whilst the dependence of methanogenesis on temperature and substrate govern the overall emission magnitude (Eq. 12), they do not determine the peak location (though this would change if vertical temperature gradients were incorporated).

Given the functional forms of $f_w^{(p)}$, $f_w^{(o)}$, and k_e (see Sect. 2), Eq. (15) involves a mixture of exponential and polynomial terms and must be solved numerically for $z_w = z_p$. For $z_w < z_s$, we have $df_e^*/dz_w > 0$ for typical parameter ranges and Eq. (15) cannot be satisfied, so peak emissions must always occur at or above the soil surface. For $z_w > z_s$ Eq. (15) yields

$$\frac{-2D}{(z_w - z_b)^3}\left(k_o f_T^{(o)} e^{-p_2(z_w - z_b)} + k_{EP} + \frac{D}{(z_w - z_b)^2}\right) + k_e p_2 k_o f_T^{(o)} e^{-p_2(z_w - z_b)}$$
$$-\frac{k_e p_1}{z_w - z_b}\left(k_o f_T^{(o)} e^{-p_2(z_w - z_b)} + k_{EP} + \frac{D}{(z_w - z_b)^2}\right) + \frac{2Dk_e}{(z_w - z_b)^3} = 0, \tag{16}$$

or, alternatively:

$$k_o f_T^{(o)}\left[k_e\left(p_2 - \frac{p_1}{z_w - z_b}\right) - \frac{2D}{(z_w - z_b)^3}\right]e^{-p_2(z_w - z_b)} - \frac{k_{EP}}{z_w - z_b}\left[p_1 k_e + \frac{2D}{(z_w - z_b)^2}\right]$$
$$+\frac{D}{(z_w - z_b)^3}\left[(2 - p_1)k_e - \frac{2D}{(z_w - z_b)^2}\right] = 0. \tag{17}$$

Whilst one could in principle solve Eq. (17) directly to obtain the depth of peak emissions, the specific functional form of k_e given in Eq. (9) (see also Fig. 1c) simplifies the analysis. For $z_w > z_s$, the derivative satisfies $dk_e/dz_w \approx 0$, so the first term on the left-hand side of Eq. (15) can be neglected. A practical approximation is therefore obtained by solving the more interpretable equation

$$k_o f_T^{(o)}\left(p_2 - \frac{p_1}{z_w - z_b}\right)e^{-p_2(z_w - z_b)} - \frac{p_1 k_{EP}}{z_w - z_b} + \frac{(2 - p_1)D}{(z_w - z_b)^3} = 0. \tag{18}$$

The accuracy of this reduced formulation is illustrated in Fig. 7 (red crosses), which shows excellent agreement with solutions to Eq. (17) (black lines).

The existence of a positive root requires that the sum of the positive terms outweighs the negative ones for $z_w > z_s$; otherwise, provided $p_1 \neq 0$, emissions are maximised at the soil surface (i.e. $z_p = 0$). These dependencies may be able to explain conflicting conclusions for optimal water depth for emissions. For example, Zhang et al. (2024) report exponential decay in CH_4 emission fluxes with water depth above the surface, which contrasts with the data synthesis performed by Calabrese et al. (2021); this may result from stronger oxidation or weaker plant transport in the wetlands studied by Zhang et al. (2024). Similarly, Taylor et al. (2023) report that water depth for peak emissions depends on the wetland type (e.g. bog vs. fen).

5.2 Critical water depth dependence on model parameters

Eq. (18) reflects a balance of competing effects: the exponential decline in oxidation against the hyperbolic decay in production with depth (first term), plant-mediated transport (second term), and diffusion (third term). Since the diffusion term depends

https://doi.org/10.5194/egusphere-2025-6013
Preprint. Discussion started: 12 December 2025

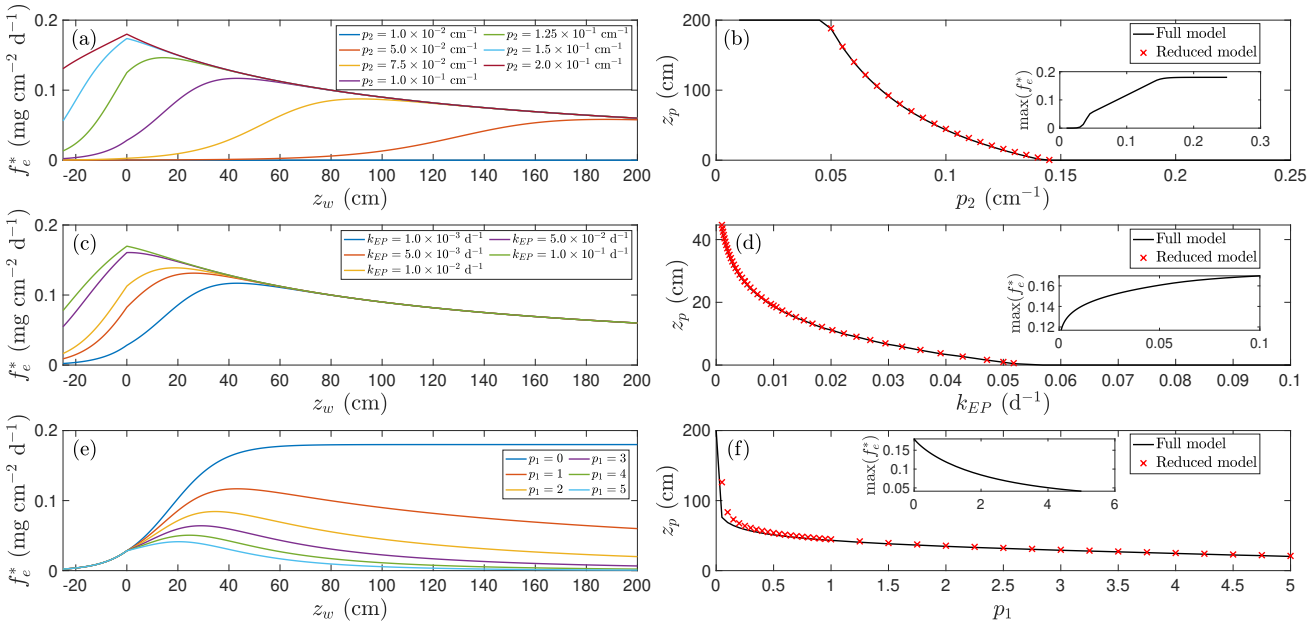

Figure 7. Relationship between CH_4 emissions and water table depth for different parameter families. Panels (a,b) show effect of varying p_2, panels (c,d) show effect of varying k_{EP} and panels (e,f) show effect of varying p_1. Left panels (a,c,e) show representative solutions, right panels (b,d,f) show location of emission peak as a function of varied parameter (insets show magnitude of this peak). Red crosses indicate approximation found by solving Eq. (18). Unless otherwise indicated parameters are $k_p = 1.0$ mg CH_4 cm^{-2} d^{-1}, $p_1 = 1.0$, $k_o = 2.0 \times 10^2$ d^{-1}, $p_2 = 1.0 \times 10^{-1}$ cm^{-1}, $Q_p = 5.0$, $p_3 = 1$, $Q_o = 1.5$, $z_b = -1.0 \times 10^{-2}$ cm, $k_{EP} = 1.0 \times 10^{-2}$ d^{-1}, $p_5 = 2.0$, $T = 20°$C and NDVI = 0.8.

strongly on depth, its relative influence diminishes when $z_w - z_b$ is large. Furthermore, if $p_1 > 2$ and $p_1 > (z_w - z_b)p_2$, no positive solution exists and emissions peak at the surface, driven by the rapid decline in production with depth. Other parameter combinations can also preclude a solution, depending on how oxidation is modulated by temperature and other environmental factors (see discussion in Sect. 5.3).

We explore these dependencies in Fig. 7, which shows, for fixed baseline parameters, the influence of (a,b) the oxidation decay rate, (c,d) plant transport and ebullition, and (e,f) production decay on peak emission depth. The chosen parameters correspond to those identified as influential by means of a Morris sensitivity analysis (App. B). Figs. 7(a,c,e) display representative CH_4 flux curves for different parameter families, whilst panels (b,d,f) plot the associated peak depths (insets show the corresponding maximum emission rate).

The physical interpretation follows directly from the functional forms in Fig. 1. Methane production is highest at the soil surface, rising as the water table approaches the surface as more of the soil column is exposed to anoxic conditions favourable to methanogenesis but declining when the soil column becomes deeply inundated because of substrate dilution. In contrast, oxidation decreases exponentially with depth and diffusive release scales approximately as an inverse square of water depth.

https://doi.org/10.5194/egusphere-2025-6013
Preprint. Discussion started: 12 December 2025

When the oxidation decay rate p_2 increases, the aerobic oxidation zone quickly collapses with water depth and CH_4 is consumed less efficiently. As a result, the emission peak shifts upward toward the soil surface and the total flux rises by orders of magnitude (Fig. 7a–b). At the extreme of large p_2 the model predicts almost no oxidation, so production nearly completely controls the flux and the peak coincides with the soil surface (Figs. 7a-b); in particular, in this regime deep inundation is not required to limit CH_4 consumption.

Meanwhile, increasing plant-mediated transport and ebullition produces a similar but more modest effect, shifting both the location and magnitude of the emission peak. Greater ebullition and plant transport allow CH_4 to rapidly bypass the oxic layer, further reducing the role of oxidation. Since these pathways are largely independent of water depth, and diffusion is weak above the surface, the overall flux pattern is increasingly determined by the near-surface production profile: higher transport rates both increase emission magnitude and move the peak closer to the surface (Fig. 7c–d), as transport outcompetes oxidation of CH_4 produced in the soil column. In particular, as the dominant emission pathway shifts from diffusion, which decays with water depth, to constant ebullition and plant transport, emissions become more directly governed by production. Wetlands with abundant emergent vegetation therefore tend to exhibit higher fluxes and shallower emission peaks. As these emission routes depend directly on the total CH_4 present in the soil column, a reinforcing feedback occurs: higher emissions deplete CH_4 available for future release, further shifting the peak toward the soil surface where production is maximal.

The influence of production decay is subtler in magnitude but far more significant for peak location. For instance, when $p_1 = 0$, peak emissions occur at $z_w \to \infty$, with emissions effectively plateauing with increasing inundation, consistent with the absence of depth-dependent decline in production and continued loss of CH_4 via oxidation (this balance can also be readily observed in Eq. 18, which becomes strictly positive). As p_1 increases, deeper water no longer offsets oxidation because production itself is suppressed; the emission maximum therefore migrates toward the soil surface (Fig. 7e–f). This behaviour can also be inferred from the simplified analytical condition (Eq. 18), which becomes strictly positive when $p_1 = 0$.

These results explain why a deeper wetland can sometimes emit less CH_4 than a shallower one when oxidation remains active, whereas wetlands rich in organic carbon, such as agricultural systems, can become largely anoxic and release much more CH_4. They also show that increasing plant-mediated transport, ebullition, or substrate availability consistently raises emissions and shifts the peak toward the soil surface. In contrast, extending the oxidation decay length suppresses fluxes by enlarging the aerobic consumption zone.

5.3 Critical water depth dependence on temperature

A notable consequence of Eq. (17) is that the peak location is itself temperature-dependent via $f_T^{(o)}$, implying that both the magnitude and position of peak emissions shift throughout the growing season in response to a shifting balance between production and oxidation. Figure 8 illustrates this dependence: panel (a) shows CH_4 fluxes at fixed temperatures, whilst panel (b) plots the corresponding peak emission depths and flux magnitudes. As temperature increases, both the intensity of emissions and the depth at which they peak typically rise, shifting the emission maximum further above the soil surface. This behaviour reflects the fact that warming generally amplifies CH_4 production throughout the inundated column more strongly than it enhances oxidation (see also Fig. 6), so that the net flux maximum tends to occur at progressively higher positions above the

https://doi.org/10.5194/egusphere-2025-6013
Preprint. Discussion started: 12 December 2025

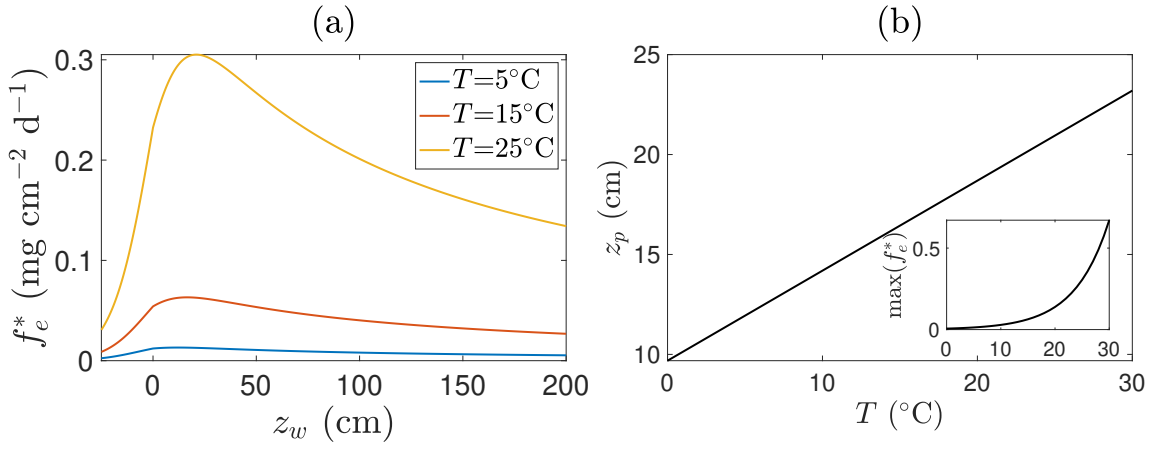

Figure 8. Relationship between CH_4 emissions and water table depth for fixed parameters and different soil temperatures. Panel (a) shows representative solutions at $T = 5°C$ (blue line), $T = 15°C$ (orange line), and $T = 25°C$ (yellow line) of steady state emissions fluxes against water table depth. Panel (b) shows location of emission peak as a function of temperature (insets show magnitude of this peak). Parameters are $k_p = 1.0$ mg CH_4 cm^{-2} d^{-1}, $p_1 = 1.0$, $k_o = 2.0\times10^2$ d^{-1}, $p_2 = 1.0\times10^{-1}$ cm^{-1}, $Q_p = 5.0$, $p_3 = 1$, $Q_o = 1.5$, $z_b = -1.0\times10^{-2}$ cm, $k_{EP} = 1.0\times10^{-2}$ d^{-1}, $p_5 = 2.0$ and NDVI $= 0.8$.

soil surface. However, under some parameter choices, in particular when $p_1 > p_2(z_w - z_b)$, the temperature-driven increase in oxidation can instead shift the peak closer to the soil surface. Since this typically occurs only when $z_w - z_b$ is small and p_1 is large, it is usually a weaker effect.

This temperature sensitivity carries broader implications. As global temperatures rise, wetlands may exhibit not only higher CH_4 emissions but also shifts in the vertical structure of those emissions. Such changes could impact the efficacy of interventions aimed at suppressing emissions, particularly those based on manipulating water levels. Optimal water levels for mitigation may vary substantially across seasons or under future climatic conditions, necessitating adaptive, site-specific strategies.

6 Discussion

In this paper we have presented a simple zero-dimensional model to describe the response of wetland CH_4 emissions to variations in water depth, temperature, and vegetation-derived substrate input. This work refines and extends the framework of Calabrese et al. (2021) by demonstrating how seasonal fluctuations in these environmental drivers modulate the balance between methanogenesis and oxidation, thereby shaping both the magnitude of peak methane emissions and the conditions under which this peak occurs. In particular, the model reveals that strong oxidative capacity within the wetland column can substantially mitigate CH_4 emissions by acting as an effective sink for produced CH_4, an effect most pronounced in temporarily inundated wetlands. The model thus provides a mechanistic basis for understanding seasonal emission patterns and assessing the combined influence of environmental controls on wetland CH_4 fluxes. Although intentionally simple, a fully mechanistic,

https://doi.org/10.5194/egusphere-2025-6013
Preprint. Discussion started: 12 December 2025

higher-dimensional representation would require detailed parameterisation and extensive process-level data. In contrast, our model offers a computationally efficient yet physically informed approach that captures the essential dependencies governing CH_4 production and emission dynamics.

A key emergent outcome of the non-linear interaction between methanogenesis, oxidation, and transport identified by our model is an intermediate critical water depth at which CH_4 emissions are maximised (such a peak has also been identified by Calabrese et al., 2021, but is inaccessible using other models based solely on subsurface water tables). Although derived under a steady-state assumption, this analysis provides valuable insight into system behaviour at intermediate times, particularly because the governing ODEs are linear in CH_4 pool size. We isolate the key parameters controlling both the magnitude and position of this emission peak – specifically, the exponential decay of oxidation, the hyperbolic decay of production, plant-mediated transport and ebullition, and diffusion. We examine how these processes interact to shape emission profiles (see Fig. 7), complemented by a global sensitivity analysis in App. B. Importantly, we show that in some wetlands the depth of peak emissions is temperature-dependent, reflecting the modulation of oxidation rates by seasonal temperature changes. This indicates that optimal water levels for maximal CH_4 fluxes can vary over the growing season or under different climate scenarios, highlighting the potential necessity for seasonally adaptive management strategies.

This understanding is facilitated by the model's simple zero-dimensional structure, which provides a computationally efficient alternative to more complex, spatially explicit PDE-based models. However, limitations emerge when the water table falls below the soil surface, potentially reflecting either a breakdown of the zero-dimensional approximation in this regime or the coarse method used to estimate water depth (see Sect. 3.1). Nevertheless, emissions under these conditions are generally small compared to those during saturated or inundated periods, so any overestimation has limited impact on total seasonal budgets. Improving model performance during low-water periods would nonetheless broaden its applicability beyond wetland centres, enabling predictions across spatially heterogeneous landscapes where water table depth varies substantially with soil profile (wetland bathymetry). Such an extension would support more accurate, large-scale assessments of wetland CH_4 emissions.

Beyond water table depth, soil temperature and substrate availability, wetland CH_4 emissions are controlled by a host of additional environmental and anthropogenic factors. Alternative electron acceptors such as nitrate and sulphate can suppress emissions by supporting more energetically favourable microbial pathways. Soil pH and salinity also modulate emission pathways: acidic soils favour hydrogenotrophic methanogenesis, whilst saline coastal wetlands tend to exhibit reduced CH_4 production (Poffenbarger et al., 2011). Microbial community composition also varies between sites, with acetoclastic-dominated communities showing particularly strong seasonal responses (Angle et al., 2017). Wetland hydrology also plays an important role, with flooding duration and frequency influencing oxygen availability and nutrient loading. Similarly, wetland morphology controls emissions, with larger wetlands (i.e. those with greater wetland volume to surface area) typically exhibiting lower emissions. Anthropogenic impacts, such as drainage and pollution, further alter water levels and chemical properties. In our model, we do not explicitly account for these complexities, assuming their effects are roughly constant and encapsulated in the site-specific calibration parameter, k_p. Whilst this is a simplification, our model successfully predicts both seasonal and inter-annual variations in fluxes, capturing peaks and troughs and producing accurate estimates of total seasonal emissions (see Figs. 3-5). This performance is achieved without explicitly modelling these secondary processes, suggesting that the primary

https://doi.org/10.5194/egusphere-2025-6013
Preprint. Discussion started: 12 December 2025

drivers considered are sufficient to reproduce leading-order emission dynamics. Hence, our model provides a minimal mechanistic framework for estimating CH_4 emissions and identifying environmental conditions that favour elevated fluxes. It also facilitates emission estimates under unobserved or data-sparse environmental scenarios.

Another simplification we employ is to lump the hydrogenotrophic and acetoclastic methanogenesis pathways into a single effective production term. Whilst these pathways differ in substrate requirements and temperature sensitivities – hydrogenotrophic methanogenesis typically dominating deeper in the soil and early in the season, and acetoclastic methanogenesis prevailing near the surface later in the season – this aggregation enables the model to capture their common dependence on biomass and temperature without introducing additional complexity. However, by not resolving these pathways separately, the model cannot explicitly reproduce seasonal hysteresis effects that may arise when the dominant methanogenic pathway shifts over the growing season (Chang et al., 2019, 2021). This trade-off provides further opportunity for refinement in future work: explicitly modelling both pathways could help capture asymmetric seasonal responses in CH_4 emissions more accurately.

We have validated the model against a representative set of mid-latitude wetlands in the PPR, a sensible starting point given their ecological and hydrological diversity and the availability of extensive observational data. However, further evaluation is necessary to assess model performance in other mid-latitude regions and, critically, in tropical and high-latitude wetlands to determine its generalisability. Future model developments should incorporate biomass accumulation and decay dynamics, more realistic representations of ebullition and plant-mediated gas transport, and potentially CO_2 dynamics, which may also affect methanogenesis via hydrogenotrophic pathways. Additionally, coupling the model with a stochastic representation of water table fluctuations – driven by rainfall and evapotranspiration – would facilitate investigations into how climate change, through warming-induced increases in evapotranspiration and methanogenesis alongside elevated water tables due to intensified rainfall, may alter emission patterns. Such advancements are essential for informing future wetland management strategies. In particular, whilst soil temperature and substrate availability are difficult to manipulate, water depth can be controlled through drainage, making understanding its influence on peak emissions critical for wetland management.

Appendix A: Parameter ranges

Table A1: Optimised parameters employed in simulations for the centre of wetlands P1, P3, P8, T5, T6, T9.

Parameter	P1C1	P3C1	P8C1	T5C1	T6C1	T9C1
k_p	1.95×10^{-1}	3.39×10^{-2}	7.05	7.42	2.64×10^{1}	7.55×10^{1}
p_1	9.55×10^{-1}	0	1.36	1.21×10^{-3}	4.82×10^{-4}	1.49×10^{-3}
k_o	1.10×10^{1}	1.99×10^{2}	2.00×10^{2}	1.65×10^{2}	1.47×10^{2}	2.00×10^{2}
p_2	1.00×10^{-2}	2.53×10^{-2}	5.75×10^{-2}	4.98×10^{-2}	1.94×10^{-2}	1.87×10^{-2}
Q_p	4.35	2.50	7.97	2.85	2.91	4.19
p_3	5.00	2.50	9.46×10^{-5}	5.00	5.00	3.19

Continued on next page

https://doi.org/10.5194/egusphere-2025-6013
Preprint. Discussion started: 12 December 2025

Table A1 – continued from previous page

Parameter	P1C1	P3C1	P8C1	T5C1	T6C1	T9C1
Q_o	1.02	1.38	1.67	1.00	2.00	1.01
$-z_b$	5.41×10^1	7.71×10^1	5.00×10^1	1.46×10^2	7.32×10^1	5.42×10^1
k_{EP}	1.17	8.86×10^{-1}	6.29×10^{-2}	1.36×10^{-2}	4.66×10^{-2}	1.76
τ	30	29	30	30	16	16

In Table A2 we present the allowable parameter ranges for each model parameter employed throughout the paper based on existing literature.

Table A2: Model parameter ranges.

Parameter (units)	Minimum	Maximum	Justification
k_p (mg CH_4 cm^{-2} d^{-1})	1×10^{-2}	1×10^2	Substrate production rate. Varies with redox conditions and substrate availability. Permanent wetlands tend to have higher sulphate concentrations, suppressing methanogenesis (Dalcin Martins et al., 2017). Optimisation indicates this is a suitable range.
p_1 (N/A)	0	5	Controls the degree of mixing or redistribution of carbon substrate with depth. $p_1 = 0$ implies no mixing; larger values reflect stronger redistribution. Calabrese et al. (2021) use $p_1 = 1$, but temporary wetlands may show lower effective mixing.
k_o (d^{-1})	1×10^1	2×10^2	Oxidation rate constant. Calabrese et al. (2021) use $k_o = 200$ d^{-1} as a maximum based on empirical estimates by Bender and Conrad (1992). Lower values reflect slower oxygen consumption or limited microbial activity.
p_2 (cm^{-1})	1×10^{-2}	2×10^{-1}	Controls depth dependence of oxidation. Calabrese et al. (2021) use $p_2 = 0.1$ cm^{-1}. Sensitivity analysis indicates strong non-linear effects near this value.
Q_p (N/A)	2.5	20	Temperature dependence of CH_4 production. Zhang et al. (2002); Souza et al. (2021) use $Q_p = 3$, whilst Walter and Heimann (2000) use $Q_p = 6$. Broad literature range spans 1.3 to 28 (Van Hulzen et al., 1999; Segers, 1998; Dunfield et al., 1993).

Continued on next page

https://doi.org/10.5194/egusphere-2025-6013
Preprint. Discussion started: 12 December 2025

Table A2 - continued from previous page

Parameter	Minimum	Maximum	Justification
p_3 (N/A)	0	5	Controls sensitivity of production to biomass (NDVI) variation. High values reflect stronger carbon dependence, such as in acetoclastic-dominated wetlands.
Q_o (N/A)	1	2	Temperature dependence of CH_4 oxidation. Generally weaker than for production. Dunfield et al. (1993) report $Q_o = 1.4$–2.1; Zhang et al. (2002) assume similar values.
z_b (cm)	-150	-50	Characteristic depth below which CH_4 production is negligible. Calabrese et al. (2021) use $z_b = -100$ cm. Only the upper soil profile substantially contributes to emissions.
k_{EP} (d^{-1})	5×10^{-4}	5	Combined rate constant for non-diffusive CH_4 emissions via plant-mediated transport and ebullition. Range reflects variability in vegetation structure and bubble formation.
τ (d)	5	30	Delay between NDVI dynamics and resulting carbon substrate availability for methanogenesis. Captures temporal lag from plant growth and decay to usable substrate. Bansal et al. (2023) assume a lag of $\tau = 14$ d.
p_5 (N/A)	0	5	Exponent controlling depth dependence of production when the water table is below the surface. Higher values imply sharper decline in production with depth in unsaturated conditions.

Appendix B: Sensitivity analysis

Despite efforts to minimise the number of model parameters whilst retaining essential geochemical processes, even this simplified model remains highly parameterised. When applied across large wetland landscapes, site-specific calibration becomes impractical. Instead, it is more realistic to represent landscape heterogeneity through parameter distributions. Some parameters assumed constant may also vary over time. For instance, the CH_4 production rate k_p likely depends on salinity, which fluctuates with freshwater inputs and discharge. Parameter sensitivity is further context-dependent: under persistently high water tables, oxidation parameters may have little effect, whereas under drier conditions they can dominate. Given this complexity, understanding which parameters most strongly influence model behaviour is therefore critical, particularly since several remain poorly constrained in the literature.

https://doi.org/10.5194/egusphere-2025-6013
Preprint. Discussion started: 12 December 2025

B1 Morris method

To assess the sensitivity of our model outputs to input parameters, we employ the Morris method, a global screening technique well-suited to computationally expensive models. This method efficiently identifies parameters that exert significant influence on the output, exploring the parameter space broadly by evaluating many one-at-a-time perturbations across multiple regions of the domain.

A detailed description of the Morris method is provided in Morris (1991); Stadt and Layton (2024); here we summarise the key steps. Let $f(X_1, X_2, \ldots, X_n)$ denote the model output for the parameter set $(X_1, X_2, \ldots, X_n)$. All parameters are rescaled to the unit interval $[0,1]$ and discretised into p levels, with perturbation step $\delta = 1/(p-1)$. In subsequent simulations each parameter is varied within $\pm 25\%$ of its baseline dimensional value, and the perturbations in the rescaled space are mapped back to dimensional units before evaluation.

Starting from an initial parameter set, the model is sequentially perturbed in one parameter at a time to compute the elementary effects:

$$EE_i = \frac{f(X_1, \ldots, X_i + \Delta_i, \ldots, X_n) - f(X_1, \ldots, X_i, \ldots, X_n)}{\Delta_i}, \tag{B1}$$

repeating the process for all n parameters across r random trajectories ($r = 100$ in this study). From the ensemble of $EE_i^{(k)}$ values, the sensitivity indices are computed as

$$\mu_i = \frac{1}{r}\sum_{k=1}^{r} EE_i^{(k)}, \quad \mu_i^* = \frac{1}{r}\sum_{k=1}^{r} |EE_i^{(k)}|,$$
$$\sigma_i = \sqrt{\frac{1}{r}\sum_{k=1}^{r}(EE_i^{(k)} - \mu_i)^2}, \quad M_i = \sqrt{\mu_i^2 + \sigma_i^2}. \tag{B2}$$

representing the mean, mean absolute, standard deviation, and combined Morris index, respectively; μ_i^* indicates the overall importance of parameter X_i, whilst σ_i reflects interaction or non-linearity.

To facilitate comparison across parameters of different magnitudes, we also apply the relative Morris method, in which each elementary effect is normalised by its baseline value:

$$EE_i^r = \frac{X_i}{f(X_1, \ldots, X_n)}, EE_i, \tag{B3}$$

yielding corresponding statistics μ_i^{r*}, σ_i^r, and M_i^r. This formulation expresses the response as a fractional change in output relative to a fractional change in input, allowing fairer comparison across parameters. We report both absolute and relative indices to identify parameters with the greatest absolute or proportional influence on model output.

B2 Sensitivity of emission fluxes to parameters

We assess the sensitivity of steady-state CH_4 emission fluxes to model parameters in Fig. A1. Under fixed environmental conditions (NDVI$= 0.5$, $T = 15$°C, and $z_w = 25$ cm), Fig. A1(a) shows results from both the absolute and relative (normalised)

https://doi.org/10.5194/egusphere-2025-6013
Preprint. Discussion started: 12 December 2025

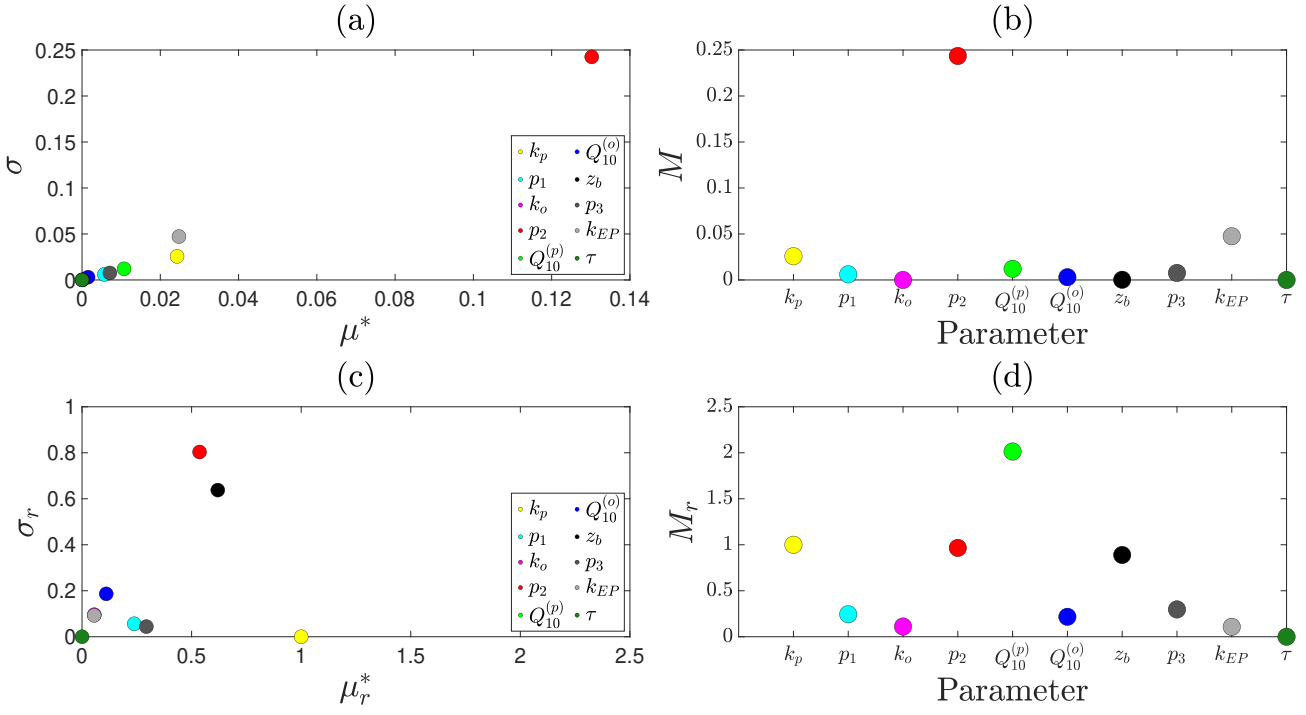

Figure A1. Sensitivity analysis of predicted steady-state CH_4 emission fluxes. For a fixed water depth of 25 cm: (a) mean absolute (μ_i^*) versus standard deviation (σ_i) of elementary effects for each parameter; (b) corresponding ranked Morris indices. Panels (c) and (d) show the same results for the relative (normalised) Morris analysis.

Morris analyses. Panel (a) presents the scatter plot of σ against μ^* for each parameter, whilst Fig. A1(b) shows the corresponding Morris index; panels (c) and (d) present the relative counterparts.

At this moderate water table depth, the dominant absolute controls on CH_4 emissions are the decay rate of oxidation with water table depth, followed by the ebullition and plant-mediated transport rates. These parameters primarily govern the pathways through which CH_4 escapes the soil column, rather than its production. This is consistent with the relatively weak hyperbolic decay of production with water table depth compared to the sharp exponential decline in oxidation with increasing inundation. In contrast, the relative Morris analysis highlights a different picture: $Q_{10}^{(p)}$ emerges as a key control on CH_4 dynamics, reflecting its strong influence on temperature-dependent methanogenesis under these moderate conditions. Secondary relative sensitivities are found for k_p, p_2, and z_b, which together regulate CH_4 production, oxidation, and the effective soil volume available for methanogenesis. These collectively shape both the magnitude and spatial extent of CH_4 generation and oxidation within the soil column.

To explore how parameter sensitivities change across hydrological regimes, we examine absolute and relative Morris indices for each parameter across water table depths from 25 cm below to 200 cm above the soil surface (Fig. A2). A clear transition emerges in the dominant controls on CH_4 emissions. When the water table is below the soil surface, aerobic conditions favour

https://doi.org/10.5194/egusphere-2025-6013
Preprint. Discussion started: 12 December 2025

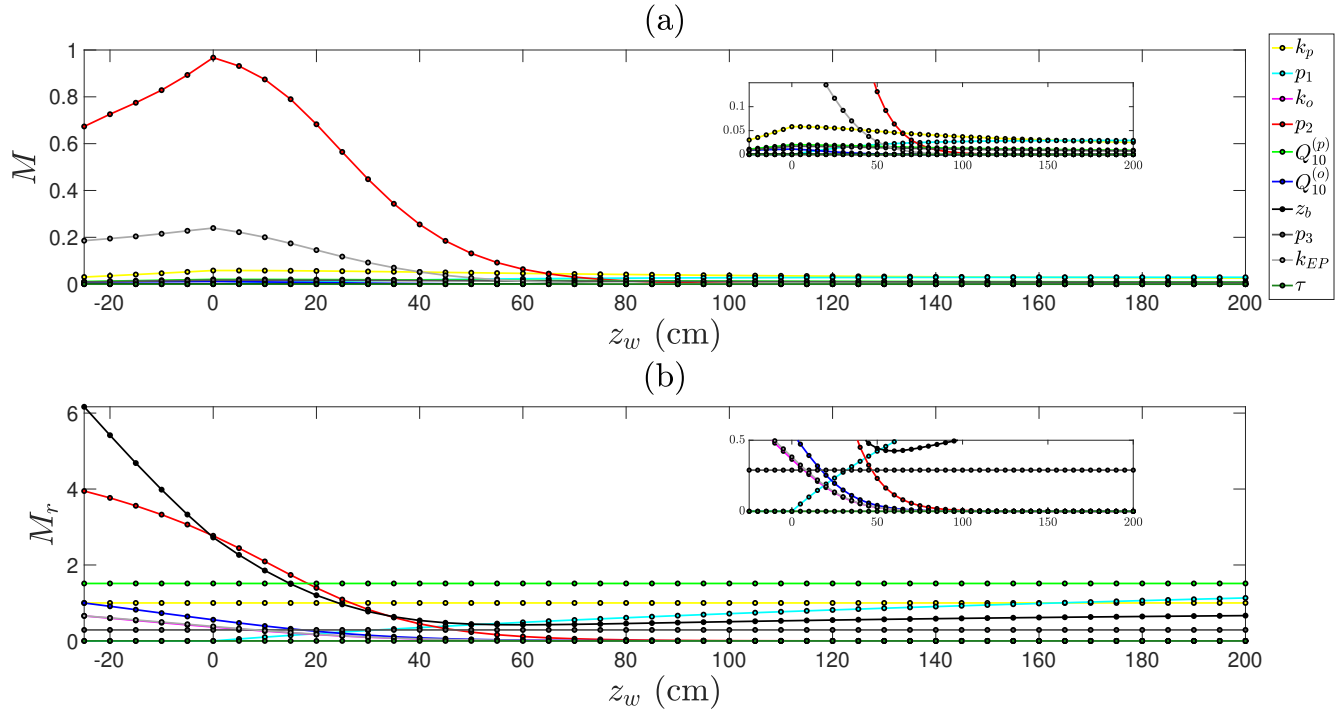

Figure A2. Sensitivity analysis of predicted steady-state CH_4 emission fluxes across water table depths, with constant NDVI and temperature. (a) Absolute Morris indices and (b) relative (normalised) Morris indices for each parameter as a function of water depth.

oxidation, and sensitivity is highest to the oxidation decay rate (p_2) and the constant emission rate from the soil column (k_{EP}). As the water table rises above the surface, the influence of oxidation declines sharply; under anaerobic conditions, CH_4 largely escapes unoxidised, rendering oxidation dynamics negligible (see insets in Fig. A2). Under these inundated conditions, emissions are instead controlled by methanogenesis and transport parameters, particularly ebullition and plant-mediated flux rates, and the hyperbolic decay term in CH_4 production, which has no effect when the water table lies below the surface. The relative Morris analysis (Fig. A2b) additionally highlights the dominant role of the contributing soil depth (z_b), which determines the volume of soil participating in production, oxidation, and emission, and is therefore consistently influential when the water table is near or below the surface. Under deeper water table conditions, CH_4 production in the soil column becomes the primary determinant of emissions. In this regime, the top three controls are $Q_{10}^{(p)}$, p_1, and k_p, reflecting strong temperature sensitivity, the production decay with water table depth, and the base production rate. Produced CH_4 is largely released at a constant rate via plant-mediated transport and ebullition.

Overall, the sensitivity analysis highlights how the dominant controls on CH_4 emissions shift with hydrological regime and demonstrate the need to prioritise accurate representation of different parameters under these regimes. When the water table lies near or below the soil surface, oxidation-related parameters are most critical, whereas production-related parameters dominate when the water table is high above the soil surface.

https://doi.org/10.5194/egusphere-2025-6013
Preprint. Discussion started: 12 December 2025

Code and data availability. This study did not generate experimental data. All numerical data used to produce the figures were generated using MATLAB 2025B. The code required to reproduce these figures is available at https://github.com/gmcnicol1/Wetland_emissions_model, with a permanent DOI https://doi.org/10.5281/zenodo.17795563. Methane flux and environmental covariate data used to validate the model were obtained from the USGS data release "Methane flux model for wetlands of the Prairie Pothole Region of North America: Model input data and programming code" (Bansal and Tangen, 2022). We thank the original authors for making these data publicly available.

Author contributions. All authors have made substantial intellectual contributions to the study conception, execution, and design of the work. All authors have read and approved the final manuscript. In addition, the following specific contributions occurred: Conceptualisation: ATL, and NBB; Methodology: GRM, ATL, and NBB; Formal analysis and investigation: GRM; Writing - original draft preparation: GRM; Writing - review and editing: ATL and NBB; Funding acquisition: ATL and NBB; Supervision: ATL and NBB.

Competing interests. The authors declare that they have no conflict of interest.

Acknowledgements. This work was supported by an NSERC Discovery Grant (RGPIN-2025-03958) awarded to ATL, and by funding to NBB from Environment and Climate Change Canada (Solutionscapes), the NSERC Alliance program, and as the Canada Research Chair in Global Water Sustainability and Ecohydrology. GRM was supported through these supervisory grants.

https://doi.org/10.5194/egusphere-2025-6013
Preprint. Discussion started: 12 December 2025

References

Angle, J. C., Morin, T. H., Solden, L. M., Narrowe, A. B., Smith, G. J., Borton, M. A., Rey-Sanchez, C., Daly, R. A., Mirfenderesgi, G., Hoyt, D. W., et al.: Methanogenesis in oxygenated soils is a substantial fraction of wetland methane emissions, Nat. Commun., 8, 1567, https://doi.org/10.1038/s41467-017-01753-4, 2017.

Arah, J. and Stephen, K. D.: A model of the processes leading to methane emission from peatland, Atmos. Environ., 32, 3257–3264, https://doi.org/10.1016/S1352-2310(98)00052-1, 1998.

Bansal, S. and Tangen, B.: Methane flux model for wetlands of the Prairie Pothole Region of North America: Model input data and programming code, U.S. Geological Survey data release, https://doi.org/10.5066/P9PKI29C, 2022.

Bansal, S., Tangen, B., and Finocchiaro, R.: Temperature and hydrology affect methane emissions from prairie pothole wetlands, Wetlands, 36, 371–381, https://doi.org/10.1007/s13157-016-0826-8, 2016.

Bansal, S., Johnson, O. F., Meier, J., and Zhu, X.: Vegetation affects timing and location of wetland methane emissions, J. Geophys. Res. Biogeosci., 125, e2020JG005 777, https://doi.org/10.1029/2020JG005777, 2020.

Bansal, S., Post van der Burg, M., Fern, R. R., Jones, J. W., Lo, R., McKenna, O. P., Tangen, B. A., Zhang, Z., and Gleason, R. A.: Large increases in methane emissions expected from North America's largest wetland complex, Sci. Adv., 9, eade1112, https://doi.org/10.1126/sciadv.ade1112, 2023.

Bender, M. and Conrad, R.: Kinetics of CH4 oxidation in oxic soils exposed to ambient air or high CH4 mixing ratios, FEMS Microbiol. Lett., 101, 261–270, https://doi.org/10.1111/j.1574-6941.1992.tb01663.x, 1992.

Bradford, A.: Averting degradation of southern Ontario wetlands due to hydrologic alterations associated with development, Can. Water Resour. J., 41, 543–553, https://doi.org/10.1080/07011784.2015.1119061, 2016.

Bridgham, S. D., Megonigal, J. P., Keller, J. K., Bliss, N. B., and Trettin, C.: The carbon balance of North American wetlands, Wetlands, 26, 889–916, https://doi.org/10.1672/0277-5212(2006)26[889:TCBONA]2.0.CO;2, 2006.

Bridgham, S. D., Cadillo-Quiroz, H., Keller, J. K., and Zhuang, Q.: Methane emissions from wetlands: biogeochemical, microbial, and modeling perspectives from local to global scales, Glob. Change Biol., 19, 1325–1346, https://doi.org/10.1111/gcb.12131, 2013.

Calabrese, S., Garcia, A., Wilmoth, J. L., Zhang, X., and Porporato, A.: Critical inundation level for methane emissions from wetlands, Environ. Res. Lett., 16, 044 038, https://doi.org/10.1088/1748-9326/abedea, 2021.

Chang, K.-Y., Riley, W. J., Brodie, E. L., McCalley, C. K., Crill, P. M., and Grant, R. F.: Methane production pathway regulated proximally by substrate availability and distally by temperature in a high-latitude mire complex, J. Geophys. Res. G: Biogeosciences, 124, 3057–3074, https://doi.org/10.1029/2019jg005355, 2019.

Chang, K.-Y., Riley, W. J., Knox, S. H., Jackson, R. B., McNicol, G., Poulter, B., Aurela, M., Baldocchi, D., Bansal, S., Bohrer, G., et al.: Substantial hysteresis in emergent temperature sensitivity of global wetland CH4 emissions, Nat. Commun., 12, 2266, https://doi.org/10.1038/s41467-021-22452-1, 2021.

Conrad, R.: Contribution of hydrogen to methane production and control of hydrogen concentrations in methanogenic soils and sediments, FEMS Microbiol. Ecol., 28, 193–202, 1999.

Cui, S., Liu, P., Guo, H., Nielsen, C. K., Pullens, J. W. M., Chen, Q., Pugliese, L., and Wu, S.: Wetland hydrological dynamics and methane emissions, Commun. Earth Environ., 5, 470, https://doi.org/10.1038/s43247-024-01635-w, 2024.

https://doi.org/10.5194/egusphere-2025-6013
Preprint. Discussion started: 12 December 2025

Dalcin Martins, P., Hoyt, D. W., Bansal, S., Mills, C. T., Tfaily, M., Tangen, B. A., Finocchiaro, R. G., Johnston, M. D., McAdams, B. C., Solensky, M. J., et al.: Abundant carbon substrates drive extremely high sulfate reduction rates and methane fluxes in Prairie Pothole Wetlands, Glob. Change Biol., 23, 3107–3120, https://doi.org/10.1111/gcb.13633, 2017.

Dunfield, P., Dumont, R., Moore, T. R., et al.: Methane production and consumption in temperate and subarctic peat soils: response to temperature and pH, Soil Biol. Biochem., 25, 321–326, https://doi.org/10.1016/0038-0717(93)90130-4, 1993.

Eisenlohr, W. S.: Hydrologic investigations of prairie potholes in North Dakota, 1959-68, US Government Printing Office, 1972.

Euliss Jr, N. H., Mushet, D. M., Newton, W. E., Otto, C. R., Nelson, R. D., LaBaugh, J. W., Scherff, E. J., and Rosenberry, D. O.: Placing prairie pothole wetlands along spatial and temporal continua to improve integration of wetland function in ecological investigations, Journal of hydrology, 513, 490–503, https://doi.org/10.1016/j.jhydrol.2014.04.006, 2014.

Ferreira, C. S., Kašanin-Grubin, M., Solomun, M. K., Sushkova, S., Minkina, T., Zhao, W., and Kalantari, Z.: Wetlands as nature-based solutions for water management in different environments, Curr. Opin. Environ. Sci. Health., 33, 100 476, https://doi.org/10.1016/j.coesh.2023.100476, 2023.

Forbrich, I., Yazbeck, T., Sulman, B., Morin, T. H., Tang, A. C. I., and Bohrer, G.: Three decades of wetland methane surface flux modeling by earth system models-advances, applications, and challenges, J. Geophys. Res. G: Biogeosciences, 129, e2023JG007 915, https://doi.org/10.1029/2023JG007915, 2024.

Gedney, N., Cox, P., and Huntingford, C.: Climate feedback from wetland methane emissions, Geophys. Res. Lett., 31, https://doi.org/10.1029/2004GL020919, 2004.

Grant, R. and Roulet, N.: Methane efflux from boreal wetlands: Theory and testing of the ecosystem model Ecosys with chamber and tower flux measurements, Glob. Biogeochem. Cycles, 16, 2–1, 2002.

Haas, E., Klatt, S., Fröhlich, A., Kraft, P., Werner, C., Kiese, R., Grote, R., Breuer, L., and Butterbach-Bahl, K.: LandscapeDNDC: a process model for simulation of biosphere–atmosphere–hydrosphere exchange processes at site and regional scale, Landsc. Ecol., 28, 615–636, https://doi.org/10.1007/s10980-012-9772-x, 2013.

Hondula, K. L., DeVries, B., Jones, C. N., and Palmer, M. A.: Effects of using high resolution satellite-based inundation time series to estimate methane fluxes from forested wetlands, Geophys. Res. Lett., 48, e2021GL092 556, https://doi.org/10.1029/2021GL092556, 2021.

Joabsson, A., Christensen, T. R., and Wallén, B.: Vascular plant controls on methane emissions from northern peatforming wetlands, Trends Ecol. Evol., 14, 385–388, https://doi.org/10.1016/s0169-5347(99)01649-3, 1999.

Junk, W. J.: World wetlands classification: a new hierarchic hydro-ecological approach, Wetl. Ecol. Manag., 32, 975–1001, https://doi.org/10.1007/s11273-024-10010-7, 2024.

Laanbroek, H. J.: Methane emission from natural wetlands: interplay between emergent macrophytes and soil microbial processes. A mini-review, Ann. Bot., 105, 141–153, https://doi.org/10.1093/aob/mcp201, 2010.

Le Mer, J. and Roger, P.: Production, oxidation, emission and consumption of methane by soils: a review, Eur. J. Soil Biol., 37, 25–50, https://doi.org/10.1016/S1164-5563(01)01067-6, 2001.

Li, C.: Modeling trace gas emissions from agricultural ecosystems, Nutr. Cycl. Agroecosystems, 58, 259–276, https://doi.org/10.1023/A:1009859006242, 2000.

McNicol, G., Fluet-Chouinard, E., Ouyang, Z., Knox, S., Zhang, Z., Aalto, T., Bansal, S., Chang, K.-Y., Chen, M., Delwiche, K., et al.: Upscaling wetland methane emissions from the FLUXNET-CH4 eddy covariance network (UpCH4 v1. 0): Model development, network assessment, and budget comparison, AGU Adv., 4, e2023AV000 956, https://doi.org/doi.org/10.1029/2023AV000956, 2023.

https://doi.org/10.5194/egusphere-2025-6013
Preprint. Discussion started: 12 December 2025

Melton, J., Wania, R., Hodson, E., Poulter, B., Ringeval, B., Spahni, R., Bohn, T., Avis, C., Beerling, D., Chen, G., et al.: Present state of global wetland extent and wetland methane modelling: conclusions from a model inter-comparison project (WETCHIMP), Biogeosciences, 10, 753–788, https://doi.org/10.5194/bg-10-753-2013, 2013.

Mitsch, W. J. and Gosselink, J. G.: Wetlands, John wiley & sons, 2015.

Mitsch, W. J., Bernal, B., Nahlik, A. M., Mander, Ü., Zhang, L., Anderson, C. J., Jørgensen, S. E., and Brix, H.: Wetlands, carbon, and climate change, Landsc. Ecol., 28, 583–597, https://doi.org/10.1007/s10980-012-9758-8, 2013.

Moore, T. and Dalva, M.: The influence of temperature and water table position on carbon dioxide and methane emissions from laboratory columns of peatland soils, J. Soil Sci., 44, 651–664, https://doi.org/10.1111/j.1365-2389.1993.tb02330, 1993.

Morris, M. D.: Factorial sampling plans for preliminary computational experiments, Technometrics, 33, 161–174, https://doi.org/10.1080/00401706.1991.10484804, 1991.

Mushet, D. M., Euliss Jr, N. H., Rosenberry, D. O., LaBaugh, J. W., Bansal, S., Levy, Z. F., McKenna, O. P., McLean, K., Mills, C. T., Neff, B. P., et al.: Lessons learned from wetlands research at the cottonwood Lake study area, Stutsman County, North Dakota, 1967–2021, Tech. rep., US Geological Survey, https://doi.org/10.3133/pp1874, 2022.

Nzotungicimpaye, C.-M., Zickfeld, K., MacDougall, A. H., Melton, J. R., Treat, C. C., Eby, M., and Lesack, L. F.: WETMETH 1.0: A new wetland methane model for implementation in Earth system models, Geosci. Model Dev., 14, 6215–6240, https://doi.org/10.5194/gmd-14-6215-2021, 2021.

Poffenbarger, H. J., Needelman, B. A., and Megonigal, J. P.: Salinity influence on methane emissions from tidal marshes, Wetlands, 31, 831–842, https://doi.org/10.1007/s13157-011-0197-0, 2011.

Richardson, J. L., Arndt, J. L., and Freeland, J.: Wetland soils of the prairie potholes, Adv. Agron., 52, 121–171, https://doi.org/10.1016/S0065-2113(08)60623-9, 1994.

Salimi, S., Almuktar, S. A., and Scholz, M.: Impact of climate change on wetland ecosystems: A critical review of experimental wetlands, J. Environ. Manag., 286, 112 160, https://doi.org/10.1016/j.jenvman.2021.112160, 2021.

Saunois, M., Stavert, A. R., Poulter, B., Bousquet, P., Canadell, J. G., Jackson, R. B., Raymond, P. A., Dlugokencky, E. J., Houweling, S., Patra, P. K., et al.: The global methane budget 2000–2017, Earth Syst. Sci. Data Discuss., 2019, 1–136, https://doi.org/10.5194/essd-12-1561-2020, 2019.

Schütz, H., Schröder, P., Rennenberg, H., et al.: Role of plants in regulating the methane flux to the atmosphere, Trace gas emissions by plants, pp. 29–63, 1991.

Segers, R.: Methane production and methane consumption: a review of processes underlying wetland methane fluxes, Biogeochemistry, 41, 23–51, https://doi.org/10.1023/A:1005929032764, 1998.

Smith, B., Prentice, I. C., and Sykes, M. T.: Representation of vegetation dynamics in the modelling of terrestrial ecosystems: comparing two contrasting approaches within European climate space, Global ecology and biogeography, pp. 621–637, https://doi.org/10.1046/j.1466-822X.2001.t01-1-00256.x, 2001.

Souza, R., Yin, J., and Calabrese, S.: Optimal drainage timing for mitigating methane emissions from rice paddy fields, Geoderma, 394, 114 986, https://doi.org/10.1016/j.geoderma.2021.114986, 2021.

Stadt, M. M. and Layton, A. T.: A mathematical model of whole-body potassium regulation: Global parameter sensitivity analysis, SIAM J. Appl. Dyn. Syst., 23, 2623–2642, https://doi.org/10.1137/23M161519X, 2024.

Stewart, G. A., Sharp, S. J., Taylor, A. K., Williams, M. R., and Palmer, M. A.: High spatial variability in wetland methane fluxes is tied to vegetation patch types, Biogeochemistry, 167, 1589–1607, https://doi.org/10.1007/s10533-024-01188-2, 2024.

https://doi.org/10.5194/egusphere-2025-6013
Preprint. Discussion started: 12 December 2025

Stewart, R. E. and Kantrud, H. A.: Classification of natural ponds and lakes in the glaciated prairie region, vol. 92, US Bureau of Sport Fisheries and Wildlife, 1971.

Tang, J., Zhuang, Q., Shannon, R., and White, J.: Quantifying wetland methane emissions with process-based models of different complexities, Biogeosciences, 7, 3817–3837, https://doi.org/10.5194/bg-7-3817-2010, 2010.

Taylor, M., Bradford, M., Arnold, W., Takahashi, D., Colgan, T., Davis, V., Losos, D., Peccia, J., and Raymond, P.: Quantifying the effects sizes of common controls on methane emissions from an ombrotrophic peat bog, J. Geophys. Res. G: Biogeosciences, 128, e2022JG007 271, https://doi.org/10.1029/2022JG007271, 2023.

Thauer, R. K. and Shima, S.: Methane as fuel for anaerobic microorganisms, Ann. N. Y. Acad. Sci., 1125, 158–170, https://doi.org/10.1196/annals.1419.000, 2008.

Thauer, R. K., Kaster, A.-K., Seedorf, H., Buckel, W., and Hedderich, R.: Methanogenic archaea: ecologically relevant differences in energy conservation, Nat. Rev. Microbiol., 6, 579–591, https://doi.org/10.1038/nrmicro1931, 2008.

Turetsky, M. R., Kotowska, A., Bubier, J., Dise, N. B., Crill, P., Hornibrook, E. R., Minkkinen, K., Moore, T. R., Myers-Smith, I. H., Nykänen, H., et al.: A synthesis of methane emissions from 71 northern, temperate, and subtropical wetlands, Glob. Change Biol., 20, 2183–2197, https://doi.org/10.1111/gcb.12580, 2014.

U.S. Geological Survey: National Agriculture Imagery Program (NAIP), July 20, 2014, https://earthexplorer.usgs.gov/, https://doi.org/10.5066/F7QN651G, accessed August 2025, 2014.

Van Hulzen, J., Segers, R., Van Bodegom, P., and Leffelaar, P.: Temperature effects on soil methane production: an explanation for observed variability, Soil Biol. Biochem., 31, 1919–1929, https://doi.org/10.1016/S0038-0717(99)00109-1, 1999.

Verhoeven, J. T. and Setter, T. L.: Agricultural use of wetlands: opportunities and limitations, Ann. Bot., 105, 155–163, https://doi.org/10.1093/aob/mcp172, 2010.

Walter, B., Heimann, M., Shannon, R., and White, J.: A process-based model to derive methane emissions from natural wetlands, Geophys. Res. Lett., 23, 3731–3734, https://doi.org/10.1029/1999GB001204, 1996.

Walter, B. P. and Heimann, M.: A process-based, climate-sensitive model to derive methane emissions from natural wetlands: Application to five wetland sites, sensitivity to model parameters, and climate, Glob. Biogeochem. Cycles, 14, 745–765, https://doi.org/10.1029/1999GB001204, 2000.

Walter, K. M., Zimov, S., Chanton, J. P., Verbyla, D., and Chapin III, F. S.: Methane bubbling from Siberian thaw lakes as a positive feedback to climate warming, Nature, 443, 71–75, https://doi.org/10.1038/nature05040, 2006.

Wania, R., Ross, I., and Prentice, I.: Implementation and evaluation of a new methane model within a dynamic global vegetation model: LPJ-WHyMe v1. 3, Geosci. Model Dev. Discussions, 3, 1–59, https://doi.org/10.5194/gmd-3-565-2010, 2010.

Wu, H., Cui, H., Fu, C., Li, R., Qi, F., Liu, Z., Yang, G., Xiao, K., and Qiao, M.: Unveiling the crucial role of soil microorganisms in carbon cycling: A review, Sci. Total Environ., 909, 168 627, https://doi.org/10.1016/j.scitotenv.2023.168627, 2024.

Xu, X., Yuan, F., Hanson, P. J., Wullschleger, S. D., Thornton, P. E., Riley, W. J., Song, X., Graham, D. E., Song, C., and Tian, H.: Reviews and syntheses: Four decades of modeling methane cycling in terrestrial ecosystems, Biogeosciences, 13, 3735–3755, https://doi.org/10.5194/bg-13-3735-2016, 2016.

Ying, Q., Poulter, B., Watts, J. D., Arndt, K. A., Virkkala, A.-M., Bruhwiler, L., Oh, Y., Rogers, B. M., Natali, S. M., Sullivan, H., et al.: WetCH 4: A Machine Learning-based Upscaling of Methane Fluxes of Northern Wetlands during 2016–2022, Earth Syst. Sci. Data Discuss., 2024, 1–45, https://doi.org/10.5194/essd-17-2507-2025, 2024.

https://doi.org/10.5194/egusphere-2025-6013
Preprint. Discussion started: 12 December 2025

Yuan, K., Zhu, Q., Li, F., Riley, W. J., Torn, M., Chu, H., McNicol, G., Chen, M., Knox, S., Delwiche, K., et al.: Causality guided machine learning model on wetland CH4 emissions across global wetlands, Agric. For. Meteorol., 324, 109 115, https://doi.org/10.1016/j.agrformet.2022.109115, 2022.

Yvon-Durocher, G., Allen, A. P., Bastviken, D., Conrad, R., Gudasz, C., St-Pierre, A., Thanh-Duc, N., and Del Giorgio, P. A.: Methane fluxes show consistent temperature dependence across microbial to ecosystem scales, Nature, 507, 488–491, https://doi.org/10.1038/nature13164, 2014.

Zedler, J. B. and Kercher, S.: Wetland resources: status, trends, ecosystem services, and restorability, Annu. Rev. Environ. Resour., 30, 39–74, https://doi.org/10.1146/annurev.energy.30.050504.144248, 2005.

Zhang, J., Chen, H., Wang, M., Liu, X., Peng, C., Wang, L., Yu, D., and Zhu, Q.: An optimized water table depth detected for mitigating global warming potential of greenhouse gas emissions in wetland of Qinghai-Tibetan Plateau, Iscience, 27, https://doi.org/10.1016/j.isci.2024.108856, 2024.

Zhang, Y., Li, C., Trettin, C. C., Li, H., and Sun, G.: An integrated model of soil, hydrology, and vegetation for carbon dynamics in wetland ecosystems, Glob. Biogeochem. Cycles, 16, 9–1, https://doi.org/10.1029/2001GB001838, 2002.